



Seasonal variations of sea–air CO₂ fluxes in the largest tropical marginal sea (South China Sea) based on multiple-year underway measurements

W.-D. Zhai^{1,2}, M.-H. Dai¹, B.-S. Chen^{1,3}, X.-H. Guo¹, Q. Li¹, S.-L. Shang¹, C.-Y. Zhang¹, W.-J. Cai^{3,4}, and D.-X. Wang⁵

¹State Key Laboratory of Marine Environmental Science, Xiamen University, Xiamen 361012, China

²National Marine Environmental Monitoring Center, Dalian 116023, China

³Department of Marine Sciences, University of Georgia, Athens, GA 30602, USA

⁴School of Marine Science and Policy, University of Delaware, Newark, DE 19716, USA

⁵State Key Laboratory of Tropical Oceanography, South China Sea Institute of Oceanology, Chinese Academy of Sciences, Guangzhou 510301, China

Correspondence to: M.-H. Dai (mdai@xmu.edu.cn)

Received: 27 March 2013 – Published in Biogeosciences Discuss.: 19 April 2013

Revised: 5 October 2013 – Accepted: 23 October 2013 – Published: 29 November 2013

Abstract. Based upon 14 field surveys conducted between 2003 and 2008, we showed that the seasonal pattern of sea surface partial pressure of CO₂ ($p\text{CO}_2$) and sea–air CO₂ fluxes differed among four different physical–biogeochemical domains in the South China Sea (SCS) proper. The four domains were located between 7 and 23° N and 110 and 121° E, covering a surface area of $1344 \times 10^3 \text{ km}^2$ and accounting for $\sim 54\%$ of the SCS proper. In the area off the Pearl River estuary, relatively low $p\text{CO}_2$ values of 320 to 390 μatm were observed in all four seasons and both the biological productivity and CO₂ uptake were enhanced in summer in the Pearl River plume waters. In the northern SCS slope/basin area, a typical seasonal cycle of relatively high $p\text{CO}_2$ in the warm seasons and relatively low $p\text{CO}_2$ in the cold seasons was revealed. In the central/southern SCS area, moderately high sea surface $p\text{CO}_2$ values of 360 to 425 μatm were observed throughout the year. In the area west of the Luzon Strait, a major exchange pathway between the SCS and the Pacific Ocean, $p\text{CO}_2$ was particularly dynamic in winter, when northeast monsoon induced upwelling events and strong outgassing of CO₂. These episodic events might have dominated the annual sea–air CO₂ flux in this particular area. The estimate of annual sea–air CO₂ fluxes showed that most areas of the SCS proper served as weak to moderate sources

of the atmospheric CO₂, with sea–air CO₂ flux values of $0.46 \pm 0.43 \text{ mol m}^{-2} \text{ yr}^{-1}$ in the northern SCS slope/basin, $1.37 \pm 0.55 \text{ mol m}^{-2} \text{ yr}^{-1}$ in the central/southern SCS, and $1.21 \pm 1.48 \text{ mol m}^{-2} \text{ yr}^{-1}$ in the area west of the Luzon Strait. However, the annual sea–air CO₂ exchange was nearly in equilibrium ($-0.44 \pm 0.65 \text{ mol m}^{-2} \text{ yr}^{-1}$) in the area off the Pearl River estuary. Overall the four domains contributed $(18 \pm 10) \times 10^{12} \text{ g C yr}^{-1}$ to the atmospheric CO₂.

1 Introduction

As an important component of global carbon cycling, coastal ocean carbon has received considerable attention during the past three decades (e.g., Walsh et al., 1981; Smith and Hollibaugh, 1993; Tsunogai et al., 1999; Borges et al., 2005; Cai et al., 2006; Chen and Borges, 2009; Laruelle et al., 2010; Liu et al., 2010; Borges, 2011; Cai, 2011; Dai et al., 2013). Recent estimates of global coastal ocean sea–air CO₂ fluxes have converged to conclude that the coastal ocean is an atmospheric CO₂ sink of 0.2 to 0.4 Pg C yr⁻¹ (Pg = 10¹⁵ g; Cai et al., 2006; Chen and Borges, 2009; Laruelle et al., 2010; Liu et al., 2010; Borges, 2011; Cai, 2011; Dai et al., 2013). This current estimate is a significant change from the earlier speculation of up to 1 Pg C yr⁻¹ (Tsunogai et al., 1999), but

confirms that the coastal ocean plays a disproportionately important role in the global ocean carbon budget.

It must be pointed out that the above compilation of the global scale sea–air CO₂ fluxes in the coastal ocean is often based on snapshot measurements in individual systems. In many of these coastal systems, spatial and temporal changes in CO₂ fluxes remain to be resolved as large uncertainties are often associated with the presently reported CO₂ fluxes in individual systems, which would in turn impact on the estimation of global fluxes. From the perspective of predictability of future change, both the variation in time and space as well as the inherent controlling processes need to be better understood. Adding even more complexity is that the coastal ocean is very often characterized by the highest spatial gradient in both physics and biogeochemistry, and hence has inherited complicated and differing physical–biogeochemical domains.

The South China Sea (SCS) is a marginal sea system encompassing a large variety of physical–biogeochemical domains. The SCS proper, located between 4 and 23° N and 105 and 121° E and characterized by either a tropical or subtropical climate, has both deep basins and extensive shelf systems in the northern and southern boundaries (Fig. 1) associated with large riverine inputs. The SCS is also featured by dynamic exchange with the western Pacific Ocean via an upper part exchange with the Kuroshio and overflow at depth (Chen et al., 2001; Dai et al., 2013; Du et al., 2013). At this dynamic interface, mesoscale processes such as eddies are frequently observed. As such, enriched physical–biogeochemical domains are concentrated in the SCS (Fig. 1), which also represents the lines of the present study. We considered four contrasting physical–biogeochemical domains, and were able to significantly improve our understanding regarding the spatial variability of CO₂ fluxes.

Among these four domains, A was adjacent to the Pearl River estuary (PRE) and was thus influenced by the summer estuarine plume (Gan et al., 2009; Cao et al., 2010; Han et al., 2012). Domain B covered the slope and deep basin areas in the northern SCS, which is typically oligotrophic (Wong et al., 2007) and low in productivity (Chen and Chen, 2006). Domain C covered a large portion of the SCS basin and is characterized by a tropical oligotrophic environment (Ning et al., 2004). Domain D was located west of the Luzon Strait and was impacted by the Kuroshio intrusions, which generate various mesoscale eddies and internal waves (e.g., Li et al., 1998; Yuan et al., 2006; Chen et al., 2007a; Sheu et al., 2010a). We must point out that beyond the four domains that the present study is examining, other physical–biogeochemical processes may dominate. For example, summer coastal upwelling-induced CO₂ dynamics must be considered in the southwestern part of the Taiwan Strait, in the eastern coast off Hainan Island, and in the eastern coast off Vietnam (e.g., Zhai et al., 2009; Cao et al., 2011).

Thus far, limited data sets with different spatial coverage have suggested that the SCS proper serves as a weak or

moderate source of atmospheric CO₂ in warm seasons (Rehder and Suess, 2001; Zhai et al., 2005a; Chen et al., 2006; Zhai et al., 2009; Dai et al., 2013). In shaping this source term, at least in the basin area of the SCS, the inflow of the CO₂-enriched North Pacific deep water through the Luzon Strait and its subsequent upward transport into the thermocline through vertical mixing and upwelling may have played a critically important role (Dai et al., 2013). In contrast, based on time series observations at the SEATS (South-East Asian Time Series Study) station (18° 15' N, 115° 35' E), Chou et al. (2005), Tseng et al. (2007), and Sheu et al. (2010b) noted seasonal/interannual variability in carbon chemistry including computed sea surface partial pressure of CO₂ (*p*CO₂) between 1999 and 2008, and report that the northern SCS serves as a very weak sink of atmospheric CO₂ by extrapolating the SEATS results to the entire region.

Previous estimates of annual sea–air CO₂ fluxes in the SCS proper are either based on limited transects/stations (Zhai et al., 2005a; Chen et al., 2006) or spatially extrapolated from time-series observations at a single site (Chou et al., 2005; Tseng et al., 2007; Sheu et al., 2010b). We contend that this limited spatial coverage has hampered the better assessment of *p*CO₂ variability in the SCS (Fig. 1). In our study, we greatly improved the current coverage to the majority of the SCS proper by applying a large amount of new data sets obtained from multiple years and large-scale underway surveys, extending our mechanistic understanding of *p*CO₂ variability in this important tropical marginal sea, which is necessary before placing the SCS CO₂ flux in a global context. Based on our multiple-year measurements, we were much better positioned to provide CO₂ fluxes in the SCS proper at a resolution of seasonal levels.

2 Study area

The SCS proper in this study is bounded by the China mainland on the north and northwest sides, Vietnam on the west and southwest sides, the Sunda Shelf and Borneo on the south side, Taiwan Island on the northeast side, and the Philippines on the east side. The total area of the SCS proper, excluding the Gulf of Thailand and the Gulf of Tonkin, is estimated as approximately 2.5×10^6 km² (Fig. 1). In its northern part, climatic variations of the sea–air interface are primarily dominated by the Asian monsoon. The rain-bearing southwest monsoon lasts from June to September, but the northeast monsoon, typically with higher wind speed prevails in winter, from November to March (Han, 1998).

The center of the SCS proper is a deep basin with a maximum depth exceeding 4700 m, which is surrounded by extensive shelf systems in the northern and southern boundaries. In the east and west boundaries, however, the shelves are narrow and the slopes are steep. The SCS proper has a basin-wide cyclonic gyre in the winter and an anticyclonic gyre over the southern half in the summer (Fig. 1). The latter is usually

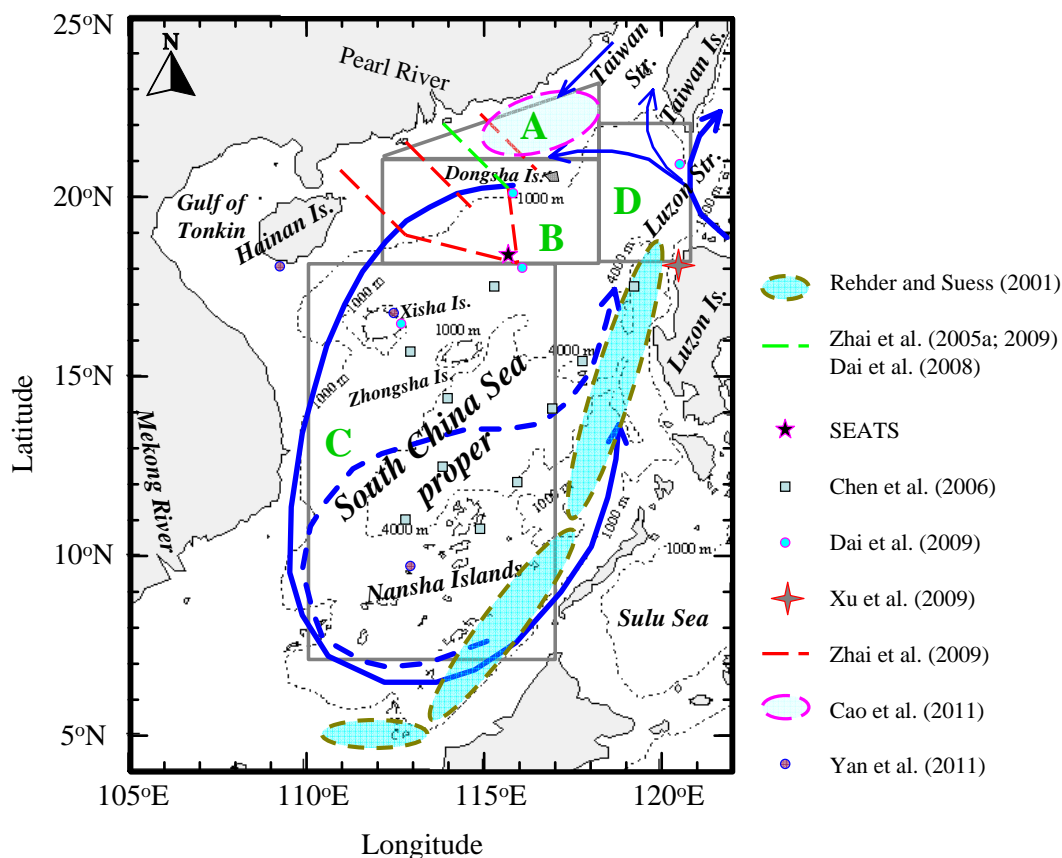


Fig. 1. Map of the South China Sea (SCS) proper under study. Framed areas indicate the four physical–biogeochemical domains this study categorized, as detailed in Table 1. Blue curves represent the basin-wide cyclonic gyre in winter (solid curve in the SCS) and the anticyclonic gyre over the southern half of the sea during the summer (dashed curve in the SCS) and the Kuroshio and its intrusions (solid curves around the Luzon Strait) into the northern SCS. All published studies related to sea–air CO₂ fluxes in the SCS proper are summarized (see the text for details). Note that the sea–air CO₂ fluxes at the SEATS station have been well studied in Chou et al. (2005), Tseng et al. (2007), and Sheu et al. (2010b).

associated with an eastward jet off the coast of Vietnam. The northern SCS also exchanges with the Kuroshio via the Luzon Strait of 2000 m depth. Although the SCS shelf systems are fed by two of the world's major rivers (the Mekong and Pearl rivers) and some smaller rivers featuring either tropical or subtropical watersheds, the majority of the SCS proper is typically oligotrophic with low productivity (Ning et al., 2004; Chen and Chen, 2006; Du et al., 2013). In our study, we focused on four selected physical–biogeochemical domains in the SCS proper (Fig. 1, Table 1), where the spatial coverage of our observational data was satisfactory at a temporal resolution of seasonal levels (Fig. 2).

Among the four domains, A could absorb CO₂ from the atmosphere in the spring/summer bloom periods (Dai et al., 2008; Zhai et al., 2009; Cao et al., 2011), while during the northeast monsoon seasons it was influenced by the cooling effect and intrusion of the Kuroshio (Fig. 1). Domain B was located between 18 and 21° N and 112 and 118° E. Zhai et al. (2005a) suggest that most of the sea sur-

face *p*CO₂ in this domain is dependent on sea surface temperature (SST) following a simple exponential equation of $(370 \pm 20 \mu\text{atm}) \times e^{0.0423 (SST - 26)}$. Domain C was located between 7 and 18° N and 110 and 117° E. As the deep basin of the SCS, its upper mixed layer is shallow all the year round. Both mesoscale eddies and the Mekong River plume have impacts on the southwestern part of this domain during the southwest monsoon period (e.g., Chen et al., 2010; Hu et al., 2011). However, regionally averaged primary production and sea surface chlorophyll concentrations vary within limited ranges (Tan and Shi, 2009; Sasai et al., 2013). On the other hand, due to abundant coral reefs on Nansha, Xisha, and Zhongsha islands, this domain was potentially influenced by CaCO₃ formation, which releases CO₂ into the atmosphere (Dai et al., 2009; Yan et al., 2011). Domain D was located between 18 and 21° N and 118 and 121° E, where the Kuroshio intrusions generate mesoscale cyclonic eddies in the northeast monsoon season (Sheu et al., 2010a) and thus induce pumping/entrainment of nutrients and CO₂ from the

Table 1. Physical–biogeochemical domains in the South China Sea categorized in the present study.

Domain #	Domain name/description	Characteristics	Latitude (° N)	Longitude (° E)	Area (10 ³ km ²)	Surveying months
A	Off the Pearl River estuary	Summer river plume, winter cooling	21–23	112–118	68	Oct 2003, Feb 2004, May 2004, Jul 2004, Sep 2004, Apr 2005, Feb 2006, Oct 2006, Nov 2006, Dec 2006, Jul 2007, Sep 2007
B	Northern basin (including the northern slope area)	Oligotrophic, winter cooling	18–21	112–118	209	Oct 2003, Feb 2004, May 2004, Jul 2004, Sep 2004, Apr 2005, Feb 2006, Oct 2006, Nov 2006, Dec 2006, Jul 2007, Sep 2007
C	Central and southern basin	Oligotrophic, warm all the year round, coral reefs	7–18	110–117	928	Oct 2003, May 2004, Apr 2005, Dec 2006, Jul 2007, Aug 2007, Sep 2007
D	West of the Luzon Strait	Oligotrophic, cold eddies in winter	18–22	118–121	139	Sep 2004, Dec 2006, Jul 2007, Apr 2008

depths (e.g., Xu et al., 2009; Shang et al., 2012; Sasai et al., 2013). The total area of the four domains was estimated as $1344 \times 10^3 \text{ km}^2$, accounting for $\sim 54\%$ of the SCS proper (Fig. 1).

3 Sampling and methods

Between October 2003 and April 2008, a total of 14 cruises (Table 2) were made aboard the following vessels: R/V *Shiyan 3* (October 2003, May 2004, and September 2004), R/V *Yanping 2* (February 2004 and July 2004), R/V *Haijian 83* (February 2006), R/V *Kexue 3* (October 2006), and R/V *Dongfanghong 2* (the rest). During these cruises, except for September 2004, quasi-surface water was continuously pumped into instruments for analysis from a side intake at a depth of 2 to 3 m (for R/V *Yanping 2* and R/V *Kexue 3*) or 4 to 5 m (for R/V *Shiyan 3*, R/V *Haijian 83*, and R/V *Dongfanghong 2*). Sampling sites/cruise tracks are presented in Fig. 2. During the September 2004 survey (Fig. 2g), surface water at 0.5 to 1 m depth was pumped up and measured for 30 min at every station. In February 2006, a parallel study was carried out at and around the Xisha Islands (i.e., Dai et al., 2009), and the data measured underway (5 to 10 nautical miles off the islands) are also plotted in Fig. 2b. During the continuous/discrete pumping, the temperature, salinity, and $p\text{CO}_2$ of the seawater were continuously measured and recorded. Note the July 2004 cruise (Fig. 2e) has been described in Zhai et al. (2009) and some of the data collected in February 2004 (Fig. 2a) have been reported in Jo et al. (2012); see Table 2 for details.

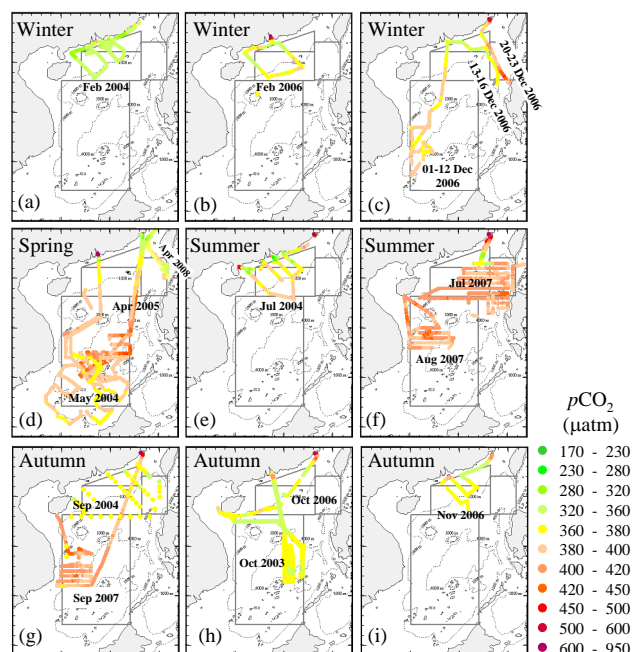


Fig. 2. Sampling sites and spatial distributions of sea surface $p\text{CO}_2$ during mapping surveys conducted between October 2003 and April 2008. The legends for (a) to (i) are the same.

3.1 Temperature and salinity determination

During the cruises, the temperature and salinity of the pumped seawater were continuously measured using either a SEACAT thermosalinograph system (CTD, SBE21, Sea-Bird Co., USA) (February 2004 and July 2004), a set of Idronaut Multiparameter “Flow Through” sensor modules (IDRONAUT S.r.l., Italy) (April 2008), or a YSI 6600 meter

Table 2. Summary of the information of the sampling cruises between 2003 and 2008.

Surveying time	Domain coverage	Seasonal coverage	Sampling depth and R/V	Sampler configuration	Refs.
Oct 2003	A, B, C	Autumn	5 m (<i>Shiyan 3</i>)	Modified from Zhai et al. (2005b)	This study
Feb 2004	A, B	Winter	2 m (<i>Yanping 2</i>)	Modified from Zhai et al. (2005b)	This study*
May 2004	A, B, C	Spring	5 m (<i>Shiyan 3</i>)	Modified from Zhai et al. (2005b)	This study
Jul 2004	A, B	Summer	2 m (<i>Yanping 2</i>)	Modified from Zhai et al. (2005b)	Zhai et al. (2009)
Sep 2004	A, B, D	Autumn	1 m (<i>Shiyan 3</i>)	Modified from Zhai et al. (2005b)	This study
Apr 2005	A, B, C	Spring	5 m (<i>Dongfanghong 2</i>)	Modified from Zhai et al. (2005b)	This study
Feb 2006	A, B	Winter	5 m (<i>Haijian 83</i>)	Modified from Zhai et al. (2005b)	This study
Oct 2006	A, B	Autumn	3 m (<i>Kexue 3</i>)	Modified from Jiang et al. (2008)	This study
Nov 2006	A, B	Autumn	5 m (<i>Dongfanghong 2</i>)	Modified from Jiang et al. (2008)	This study
Dec 2006	A, B, C, D	Winter	5 m (<i>Dongfanghong 2</i>)	Modified from Jiang et al. (2008)	This study
Jul 2007	A, B, C, D	Summer	5 m (<i>Dongfanghong 2</i>)	Modified from Jiang et al. (2008)	This study
Aug 2007	C	Summer	5 m (<i>Dongfanghong 2</i>)	Modified from Jiang et al. (2008)	This study
Sep 2007	A, B, C	Autumn	5 m (<i>Dongfanghong 2</i>)	Modified from Jiang et al. (2008)	This study
Apr 2008	D	Spring	5 m (<i>Dongfanghong 2</i>)	GO8050, Zhai and Dai (2009)	This study

* Some of the data collected from this cruise have been reported in Jo et al. (2012).

(Yellow Springs Instrument Co., USA) (the other cruises). All salinity data were corrected to the practical salinity scale 1978 by intercalibration testing either shortly before or during the cruises. Also based on these intercalibration tests, we estimated that all the onboard temperature sensors were consistent with the others at an error level of less than 0.1 °C. During most cruises, other than the February, July, and September cruises in 2004, SST was calculated via onboard temperature minus 0.2 °C (in cold season surveys) or 0.3 °C (in warm season surveys) based on intercomparison experiments between underway pumping measurements and vertical profile measurements at the stations. During the February 2004 and July 2004 cruises, however, SST was continuously measured using the in situ temperature sensor of the SBE21 system. During the September 2004 cruise, SST was discretely measured using another SEACAT thermosalinograph system (SBE911+, Sea-Bird Co., USA) at every station. All the continuous data were recorded every 6 to 12 s and averaged to 1 min.

3.2 Meteorological data

Meteorological data (wind speed, wind direction, and barometric pressure) were collected with an onboard weather station at 10 m above the sea surface. Data were recorded every minute. For the purpose of flux calculation, however, satellite-derived monthly mean wind speeds (QuikSCAT, level 3, <http://podaac.jpl.nasa.gov>) referenced at 10 m above the sea surface were used. NASA's Quick Scatterometer covers the region twice a day at 06:00 and 18:00 LT. The spatial resolution is 25 km. The monthly mean wind speed values for a specific domain were calculated by averaging all of those available QuikSCAT wind speed data for the month.

3.3 pCO₂ determination

During most cruises, other than the April 2008 cruise, improved systems after Zhai et al. (2005b) and/or Jiang et al. (2008) were used to measure pCO₂. During our April 2008 cruise, an automated flowing pCO₂ measuring system (GO8050, General Oceanics Inc., USA) was used (Zhai and Dai, 2009). In these systems, a Li-Cor[®] nondispersive infrared spectrometer (Li-6252 during the October 2003 and May 2004 surveys, Li-7000 during the other cruises) was used to measure dried CO₂ fractions (xCO₂) in the equilibrator and in the air (Zhai et al., 2005b; Zhai and Dai, 2009). For calibration purposes, a series of CO₂ gas standards with xCO₂ values from 138 to 967 ppmv (parts per million volumes in dry air; the same hereafter) were applied. pCO₂ was transformed from corrected xCO₂ based on barometric pressure along the transect or air pressure in the Li-7000 detector. Intercalibration testing showed that both air pressure data sets were consistent at a relative error level of less than 0.3 % (i.e., < 3 hPa). The Weiss and Price (1980) saturated water vapor pressure and the Takahashi et al. (1993) temperature effect coefficient of 4.23 % °C⁻¹ were used to calculate in situ pCO₂. The overall uncertainty of the xCO₂ measurements and pCO₂ data processing is less than 1 % (Zhai et al., 2005a; Zhai and Dai, 2009).

CO₂ concentration in the air was typically determined every 1 to 3 h in the day and every 4 h in the night. The bow intake from which atmospheric air was pumped was installed at 6 to 10 m above the water surface to avoid contamination from the ship. For the purpose of sea–air flux estimation, the air pCO₂ data were corrected to 100 % humidity at in situ SST and salinity.

3.4 Sea–air CO₂ flux estimation

The flux calculation was based on the formula $F = k \times K_H \times \Delta p\text{CO}_2$, where k is the gas transfer velocity of CO₂, K_H is the solubility of CO₂ in seawater (Weiss, 1974), and $\Delta p\text{CO}_2$ is the mean sea–air $p\text{CO}_2$ difference. A positive flux value represented the net CO₂ exchange from sea to atmosphere and a negative flux value referred to the net CO₂ exchange from atmosphere to sea. Since the k value measured on the spot in the SCS was not available, we used the Sweeney et al. (2007) empirical functions of wind speed at 10 m height (u_{10}) to calculate the value, which is a modification of Wanninkhof (1992). We also calculated the k value based on the latter so that our results would be comparable with those of most other studies.

The Sweeney et al. (2007) (S07 for short) equation is

$$k(\text{cm h}^{-1}) = 0.27 \times C2 \times (u_{10}/\text{m s}^{-1})^2 \times (Sc/660)^{-0.5}, \quad (1)$$

and the Wanninkhof (1992) (W92 for short) equation is

$$k(\text{cm h}^{-1}) = 0.31 \times C2 \times (u_{10}/\text{m s}^{-1})^2 \times (Sc/660)^{-0.5}, \quad (2)$$

where u_{10} is the satellite-derived monthly mean wind speed referenced at 10 m above the sea surface; $C2$ is the nonlinearity coefficient, assuming long-term winds followed a Raleigh (Weibull) distribution (Wanninkhof, 1992; Jiang et al., 2008); Sc is the Schmidt number of CO₂ in seawater; and 660 is the Sc value in seawater ($S=35$) at 20 °C (Wanninkhof, 1992).

Following Wanninkhof (1992) and Jiang et al. (2008), the effect of the short-term variability of wind speeds (Bates and Merlivat, 2001) over a month on the gas transfer velocity was determined using

$$C2 = (u_j^2)_{\text{mean}} / (u_{\text{mean}})^2, \quad (3)$$

where u_j is all of the available satellite-derived near-surface wind speeds (units: m s^{-1} , typically twice a day along with the spatial resolution of 25 km) in a month, the subscript “mean” is to calculate the average, and u_{mean} is the monthly mean wind speed (units: m s^{-1}). The global mean $C2$ has been estimated as 1.27 (Wanninkhof et al., 2009).

4 Results

4.1 SST and salinity

Based on data presented in Tables 3, 4, 5, and 6, seasonal variations of SST in the four domains were plotted in Fig. 3a. Survey-averaged SST varied between 22.1 ± 1.2 °C in February 2004 in domain A and 30.3 ± 0.4 °C in July 2007 in domain B (Fig. 3a). Domain A was the only area where the lowest survey-averaged SST values of less than 23 °C were observed (Table 3), while we observed the highest SST of 30.82 to 31.65 °C in all domains in July 2007. In domain C, however, the seasonal variation of SST was inconspicuous.

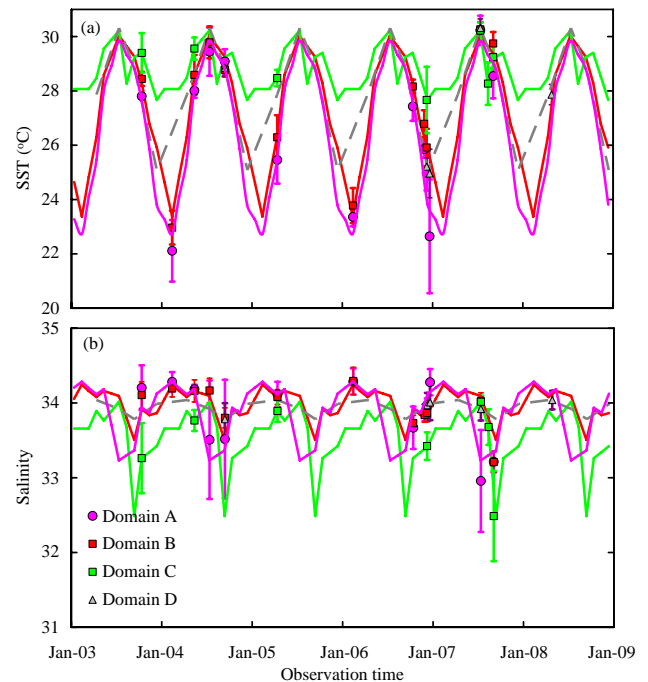


Fig. 3. Seasonal variations of sea surface temperature (SST) (a) and salinity (b) in domain A (pink curves), in domain B (red curves), in domain C (emerald green curves), and in domain D (grey dashed curves) based on data presented in Tables 3, 4, 5, and 6. Real data are shown as mean \pm standard deviation.

Very high SST values between 27.7 ± 1.3 °C in December 2006 and 30.2 ± 0.3 °C in July 2007 were observed in this domain in all seasons (Fig. 3a, Table 5).

Survey-averaged sea surface salinity varied between 32.5 ± 0.6 in September 2007 in domain C and 34.3 ± 0.2 in February 2006 in domains A and B (Fig. 3b). Most low-salinity values of < 33.5 were observed in domains A and C, which were under the influence of river plumes and/or heavy precipitation. In September 2007, the southwestern SCS is highly influenced by the Mekong River Diluted Water (MKRDW) (Chen et al., 2010). Therefore a very low sea surface salinity of 32.5 ± 0.6 was observed in domain C (Table 5). Most high-salinity values of > 34.1 were detected in domains A and B (Tables 3 and 4).

4.2 Wind speed

Survey-based mean wind speed varied between 2.2 ± 1.5 m s^{-1} in February 2006 in domain A and 17.9 ± 2.1 m s^{-1} on 21–22 December 2006 in domain D. Most field-survey mean wind speed values were lower than the monthly mean satellite-derived sea surface wind speeds (Fig. 4), presumably due to the ship contamination (Griessbaum et al., 2010) and/or the observation periods selected. Basically, the sea surface wind was stronger in northeast monsoon seasons than in southwest monsoon

seasons (Tables 3 to 6). Note that we observed a very strong wind with a two-day mean wind speed of $17.9 \pm 2.1 \text{ m s}^{-1}$ in late December 2006 in domain D, which was $\sim 50\%$ higher than the monthly mean satellite-derived sea surface wind speed (Table 6).

4.3 CO₂ concentrations in the air

Field-measured atmospheric CO₂ concentrations at 10 m ranged between 371 ± 3 ppmv in the autumns of 2003 and 2004 and 393 ± 2 ppmv in April 2008. Over the research period of 6 yr, a reasonable increasing trend was revealed (Fig. 5). In general, both seasonal and interannual variations followed the variations of atmospheric CO₂ in the North Pacific Gyre (Mauna Loa station), although terrestrial sources have been found to influence the atmospheric CO₂ at 10 m over the SCS proper, making atmospheric CO₂ concentrations here more variable than those in the open ocean. It is worth noting that relatively higher atmospheric CO₂ was observed in the northeast monsoon periods and relatively lower atmospheric CO₂ was measured in the southwest monsoon periods.

4.4 Sea surface pCO₂

In the four domains under study, sea surface pCO₂ ranged between 280 and 470 μatm (Tables 3 to 6) and mostly ranged between 320 and 420 μatm (Fig. 2). In general, sea surface pCO₂ increased southward both in individual cruises such as our 01–11 December 2006 survey (Fig. 2c) and in the composite seasonal distributions of pCO₂ based on arithmetical averages over $1^\circ \times 1^\circ$ grid boxes (Fig. 6). In domains A, B, and D, many survey-averaged sea surface pCO₂ values were fairly close to the air-equilibrated pCO₂ levels (360 to 370 μatm) (Fig. 7). In domain C, most survey-averaged sea surface pCO₂ values were quite high (Fig. 7c), although some data in October 2003 were measured as 350 to 360 μatm (Fig. 2h) and very close to the air-equilibrated pCO₂ level of this specific survey (Table 5). We note that in a parallel study in February 2006, relatively low sea surface pCO₂ of 359 to 362 μatm is also observed 5 to 10 nautical miles away from the Xisha Islands (Fig. 2b; Dai et al., 2009), which is $\sim 10 \mu\text{atm}$ lower than the nearby atmospheric pCO₂ obtained in this specific month in domain B (Table 4).

It must be pointed out that the pCO₂ variability in the SCS proper was still remarkable both in terms of time and space. For example, in domain D we observed a large variation of sea surface pCO₂ between 357 and 379 μatm on 15–16 December 2006 and between 379 and 469 μatm on 21–22 December 2006 (Table 6). The peak values of 440 to 470 μatm were observed in the 16-nautical-mile sea route around the central site at $18^\circ 42' \text{ N}$ and $119^\circ 35' \text{ E}$ (Fig. 2c). Similar to the high pCO₂ observed in domain D on 21–22 December 2006, we also measured relatively high pCO₂ of $377 \pm 17 \mu\text{atm}$ in domain A on 22–23 December 2006 (Table 3). In spring,

offshore high pCO₂ values of 420 to 463 μatm were mostly detected in domain C in April 2005 (Table 5). In summer and autumn, most relatively high pCO₂ values of 420 to 440 μatm (Table 5) were associated with the cyclonic cold eddies observed during our August–September 2007 cruise in the southwestern SCS (Chen et al., 2010; Hu et al., 2011). It should also be noted that, in the four domains, very low sea surface pCO₂ values of 280 to 320 μatm were only observed in domain A and mostly in summer (Table 3). In domain B, sea surface pCO₂ was always higher than 320 μatm (Table 4), while in domains C and D, the lowest sea surface pCO₂ was measured around 350 μatm (Tables 5 and 6).

On the other hand, interannual and/or intraseasonal variations of sea surface pCO₂ may occur (Fig. 2). For example, during our two February cruises (in winter), the sea surface pCO₂ increased approximately 20 μatm from 2004 to 2006 (Figs. 2a–b), i.e., $334 \pm 9 \mu\text{atm}$ (domain A) and $344 \pm 6 \mu\text{atm}$ (domain B) in February 2004 versus $355 \pm 4 \mu\text{atm}$ (domain A) and $367 \pm 11 \mu\text{atm}$ (domain B) in February 2006 (Tables 3 and 4). During our two July cruises (in summer), sea surface pCO₂ in domain B also increased approximately 20 μatm from 383 $\pm 11 \mu\text{atm}$ in July 2004 to $404 \pm 6 \mu\text{atm}$ in July 2007 (Table 4). In autumn, sea surface pCO₂ values averaged $365 \pm 14 \mu\text{atm}$ in domain A during most cruises other than in September 2007 (Table 3). During the latter cruise, a relatively high autumn sea surface pCO₂ value of $383 \pm 5 \mu\text{atm}$ was revealed in domain A (Table 3). In domain B, the autumn sea surface pCO₂ values ranged from $355 \pm 3 \mu\text{atm}$ in October 2003 through $364 \pm 3 \mu\text{atm}$ in September 2004 and $369 \pm 9 \mu\text{atm}$ in October–November 2006 to $383 \pm 5 \mu\text{atm}$ during the September 2007 cruise (Table 4).

Outside the four domains, sea surface pCO₂ distributions were even more dynamic especially along the southern China coastline. Except for extremely high sea surface pCO₂ of 470 to 4500 μatm in the PRE and at several coastline observation sites (Fig. 2; Zhai et al., 2005b, 2009), extremely low sea surface pCO₂ values of 230 to 280 μatm were observed in limited sea areas (Fig. 2). For example, low pCO₂ values of 234 to 280 μatm were revealed in spring in the southern Taiwan Strait and in a limited area off the PRE (Fig. 2d). The lowest pCO₂ values of 229 to 280 μatm were observed in a limited area off the PRE in July 2004 (Fig. 2e; Zhai et al., 2009).

Despite the heterogeneity of sea surface pCO₂ distributions, we can reveal distinct seasonal cycles of sea surface pCO₂ in the four domains, the composite of which is shown in Fig. 6. To summarize, nearly air-equilibrated and/or relatively low survey-averaged sea surface pCO₂ values of 330 to 350 μatm were observed in domain A in all four seasons (Table 3, Fig. 7a); in domain B, a typical seasonal cycle of CO₂ supersaturation in the warm seasons (survey-averaged pCO₂ from 383 to 404 μatm) and nearly air-equilibrated and/or relatively low averaged pCO₂ of 344 to 376 μatm in the cold seasons was revealed (Table 4, Fig. 7b); in domain C,

Table 3. Summary of $p\text{CO}_2$, salinity, and SST along cruise tracks, monthly satellite-derived wind speed, and sea–air CO₂ flux estimation in domain A. The annual sea–air CO₂ flux amounts to $-0.44 \pm 0.65 \text{ mol m}^{-2} \text{ yr}^{-1}$ using the S07 equation or $-0.51 \pm 0.75 \text{ mol m}^{-2} \text{ yr}^{-1}$ using the W92 equation. Note that $C2$ is the nonlinearity effect of the short-term variability of wind speeds over a month on the gas transfer velocity, assuming long-term winds followed a Raleigh (Weibull) distribution (Wanninkhof, 1992; Jiang et al., 2008). See text for details. Errors in sea–air CO₂ flux estimation are the temporal variability of CO₂ fluxes based on respective cruises/surveys.

Observation time	Aqueous $p\text{CO}_2$ μatm	Air $p\text{CO}_2$ μatm	Salinity	SST $^\circ\text{C}$	Wind speed m s^{-1}	$C2$	Sea–air CO ₂ fluxes ($\text{mmol CO}_2 \text{ m}^{-2} \text{ d}^{-1}$)			
							Survey average (W92)	Seasonal average (W92)	Survey average (S07)	Seasonal average (S07)
Feb 2004	334 ± 9 (315 ^a –356)	368.7 ± 3.8 (363.5–375.2)	34.28 ± 0.13 (33.97–34.52)	22.1 ± 1.2 (20.45–24.62)	9.3 ± 0.6 (7.9–10.1)	1.18	–8.59		–7.48	
Feb 2006	355 ± 4 (347–365)	370.5 ± 0.3 (370.0–371.1)	34.29 ± 0.18 (33.69–34.75)	23.4 ± 0.4 (22.65–24.05)	10.0 ± 0.4 (8.9–10.7)	1.13	–4.16		–3.63	
12–15 Dec 2006	358 ± 4 (350–371)	No data (375 ^b)	33.97 ± 0.09 (33.80–34.18)	25.0 ± 0.7 (22.90–25.72)	12.0 ± 0.5 (10.4–12.5)	1.04	–6.29	–5.6 ± 3.1 (winter)	–5.48	–4.8 ± 2.6 (winter)
22–23 Dec 2006	377 ± 18 (345–415)	381.7 ± 1.8 (378.3–385.1)	34.28 ± 0.18 (33.63–34.51)	22.6 ± 2.1 (19.42–25.36)	12.0 ± 0.5 (10.4–12.5)	1.04	–1.55		–1.35	
May 2004	379 ± 3 (374–384)	359.8 ± 1.4 (358.8–360.8)	34.18 ± 0.06 (34.07–34.29)	28.0 ± 0.3 (27.49–28.41)	5.2 ± 0.3 (4.6–5.6)	1.43	1.80		1.57	
Apr 2005	361 ± 10 (339–378)	371.0 ± 0.1 (370.9–371.1)	34.12 ± 0.17 (33.98–34.52)	25.5 ± 0.9 (23.57–26.48)	5.0 ± 0.3 (4.5–5.5)	1.43	–0.85	0.5 ± 1.9 (spring)	–0.74	0.4 ± 1.6 (spring)
Jul 2004	363 ± 26 (312–400)	361.8 ± 8.0 (356.5–373.4)	33.51 ± 0.80 (31.56–34.33)	29.4 ± 0.9 (28.01–30.92)	7.4 ± 0.3 (6.8–8.2)	1.33	0.17		0.15	
Jul 2007	350 ± 29 (281–414)	367.0 ± 1.5 (363.7–370.2)	32.96 ± 0.70 (31.89–34.40)	30.2 ± 0.6 (25.95–31.21)	5.2 ± 0.4 (4.5–5.8)	1.27	–1.49	–0.7 ± 1.2 (summer)	–1.30	–0.6 ± 1.1 (summer)
Oct 2003	365 ± 14 (349–406)	No data (355 ^c)	34.20 ± 0.30 (33.43–34.54)	27.8 ± 0.1 (27.59–27.94)	9.5 ± 0.5 (8.2–10.1)	1.12	2.49		2.17	
Sep 2004	360 ± 5 (350–364)	358.3 ± 1.4 (356.0–359.8)	33.52 ± 0.80 (33.02–33.80)	29.1 ± 0.5 (28.62–29.90)	6.2 ± 0.7 (4.7–7.3)	1.39	0.19		0.17	
Oct 2006	360 ± 8 (347–374)	363.3 ± 0.6 (362.1–364.1)	33.67 ± 0.29 (33.02–33.92)	27.4 ± 0.6 (26.71–28.41)	8.4 ± 0.6 (6.8–9.0)	1.14	–0.63	0.2 ± 2.2 (autumn)	–0.55	0.2 ± 1.9 (autumn)
Nov 2006	361 ± 6 (349–375)	369.4 ± 1.5 (367.6–372.9)	33.87 ± 0.12 (33.57–34.15)	25.9 ± 0.4 (25.14–26.59)	8.9 ± 0.3 (8.2–9.6)	1.22	–1.98		–1.72	
Sep 2007	383 ± 5 (369–396)	366.7 ± 1.7 (364.5–369.6)	33.21 ± 0.15 (32.91–33.42)	28.5 ± 0.9 (27.01–29.31)	7.5 ± 0.4 (6.9–8.4)	1.34	3.02		2.63	

^a During the cruise, low sea surface $p\text{CO}_2$ of 286 to 300 μatm was measured along the southern China coastline (Fig. 2a; Jo et al., 2012).

^b The average of the mean values measured in November 2006 and on 22–23 December 2006 in domain A.

^c The average of field-measured values in domain B in the same cruise (Table 4).

relatively high sea surface $p\text{CO}_2$ values of 360 to 425 μatm were observed all round a year (Table 5, Fig. 7c); and in domain D, $p\text{CO}_2$ was particularly dynamic in winter (Fig. 2c, Table 6).

4.5 Sea–air CO₂ flux estimation

Tables 3 to 6 summarize the sea–air CO₂ flux calculations along cruise tracks in the four domains. If we assumed that these cruise track fluxes were representative of the domains, we could obtain an overview of the seasonal variation of CO₂ sea–air exchange in the SCS proper being studied (Fig. 8). In this study, we used satellite-derived monthly averaged wind speeds and the S07 equation (Eq. 1) to calculate gas transfer velocities and then sea–air CO₂ fluxes. We also calculated sea–air CO₂ fluxes based on the W92 equation (Eq. 2) in order to better compare with other studies.

The stimulatory effect of short-term variability in wind speed on the integrated gas transfer (Bates and Merlivat, 2001) was expressed using the nonlinearity coefficient $C2$ (Eq. 3) following Wanninkhof (1992) and Jiang et al. (2008). During our study period, $C2$ varied between 1.04 (at high wind in winter) and 1.43 (at low wind in spring–summer), and this is close to the global average of 1.27 (Wanninkhof et al., 2009), although the range was slightly greater than 1.13 to 1.26 (averaged 1.18) seen on the US southeastern shelf (Jiang et al., 2008).

Tables 3 to 6 also synthesize the temporal–spatial variability of field-measured data and the estimated sea–air CO₂ fluxes. It should be noted that we reported mostly the temporal variability of CO₂ fluxes based on respective cruises/surveys in a season. If only one cruise was available, however, we reported an error based on standard deviations in wind speeds and/or the aqueous $p\text{CO}_2$. These

Table 4. Summary of $p\text{CO}_2$, salinity and SST along cruise tracks, monthly satellite-derived wind speed, and sea–air CO₂ flux estimation in domain B. The annual sea–air CO₂ flux amounts to $0.46 \pm 0.43 \text{ mol m}^{-2} \text{ yr}^{-1}$ using the S07 equation or $0.53 \pm 0.50 \text{ mol m}^{-2} \text{ yr}^{-1}$ using the W92 equation. Note that C2 and the errors in sea–air CO₂ flux estimation are the same as in Table 3. See text for details.

Observation time	Aqueous $p\text{CO}_2$ μatm	Air $p\text{CO}_2$ μatm	Salinity	SST $^\circ\text{C}$	Wind speed m s^{-1}	C2	Sea–air CO ₂ fluxes ($\text{mmol CO}_2 \text{ m}^{-2} \text{ d}^{-1}$)			
							Survey average (W92)	Seasonal average (W92)	Survey average (S07)	Seasonal average (S07)
Feb 2004	344 ± 6 (324–362)	365.6 ± 2.7 (361.4–371.1)	34.19 ± 0.12 (33.81–34.38)	23.0 ± 0.7 (21.90–24.70)	7.8 ± 0.9 (6.5–10.1)	1.19	–3.86		–3.36	
Feb 2006	367 ± 11 (342–398)	372.6 ± 2.8 (368.9–377.7)	34.29 ± 0.19 (33.78–34.75)	23.8 ± 0.7 (22.50–25.29)	8.9 ± 0.7 (7.4–10.2)	1.14	–1.28	-1.0 ± 2.3 (winter)	–1.12	-0.9 ± 1.9 (winter)
11–12 Dec 2006	376 ± 9 (357.2–393.0)	No data (375*)	33.86 ± 0.12 (33.73–34.14)	25.9 ± 0.7 (24.33–26.49)	11.9 ± 0.5 (9.7–12.9)	1.04	0.53		0.46	
May 2004	386 ± 9 (369–398)	356.9 ± 1.7 (355.5–359.4)	34.16 ± 0.15 (33.90–34.38)	28.6 ± 0.8 (26.98–29.57)	4.9 ± 0.4 (4.1–6.1)	1.49	2.57		2.24	
Apr 2005	387 ± 15 (363–444)	373.0 ± 2.6 (367.7–376.1)	34.08 ± 0.10 (33.86–34.25)	26.3 ± 0.9 (24.45–27.92)	5.2 ± 0.6 (4.1–6.5)	1.33	1.26	1.9 ± 1.0 (spring)	1.09	1.7 ± 0.8 (spring)
Jul 2004	383 ± 11 (353–417)	357.7 ± 1.1 (355.7–360.4)	34.17 ± 0.17 (33.41–34.49)	29.8 ± 0.6 (27.66–31.96)	6.9 ± 0.7 (4.7–8.3)	1.33	3.92		3.41	
Jul 2007	404 ± 6 (392–421)	366.7 ± 1.6 (362.6–370.8)	34.02 ± 0.12 (33.67–34.20)	30.3 ± 0.3 (29.09–30.96)	5.4 ± 0.5 (4.5–6.7)	1.30	3.51	3.7 ± 0.3 (summer)	3.06	3.2 ± 0.3 (summer)
Oct 2003	355 ± 3 (349–359)	354.8 ± 0.9 (354.0–356.8)	34.11 ± 0.18 (33.65–34.44)	28.4 ± 0.3 (27.88–28.83)	9.2 ± 0.8 (6.8–10.8)	1.11	0.03		0.03	
Sep 2004	364 ± 3 (360–368)	357.7 ± 1.6 (354.7–361.0)	33.80 ± 0.14 (33.47–34.06)	28.8 ± 0.3 (28.45–29.30)	6.6 ± 1.2 (4.5–8.5)	1.38	0.96		0.84	
Oct 2006	369 ± 9 (345–385)	361.5 ± 1.2 (359.8–364.8)	33.73 ± 0.11 (33.28–33.90)	28.2 ± 0.3 (27.67–28.98)	8.1 ± 1.1 (4.9–9.9)	1.18	1.42	1.2 ± 2.0 (autumn)	1.24	1.0 ± 1.8 (autumn)
Nov 2006	370 ± 5 (358–380)	370.0 ± 1.7 (366.9–374.0)	33.84 ± 0.10 (33.63–34.10)	26.8 ± 0.5 (25.35–27.50)	8.2 ± 0.7 (6.4–9.7)	1.31	–0.07		–0.06	
Sep 2007	394 ± 8 (376–411)	364.0 ± 0.8 (361.6–365.1)	33.21 ± 0.14 (32.82–33.39)	29.7 ± 0.5 (28.60–30.40)	6.5 ± 0.4 (5.5–7.7)	1.55	4.83		4.20	

* The average of the mean values measured in November 2006 and on 22–23 December 2006 in domain A (Table 3).

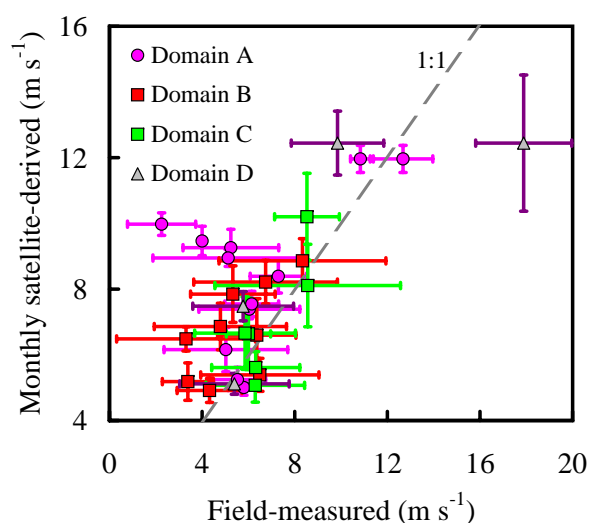


Fig. 4. Comparison between monthly satellite-derived sea surface wind speeds (QuikSCAT, level 3) and field-measured wind speeds at 10 m height. Data are shown as mean \pm standard deviation. The 1 : 1 relationship is shown as grey dashed line.

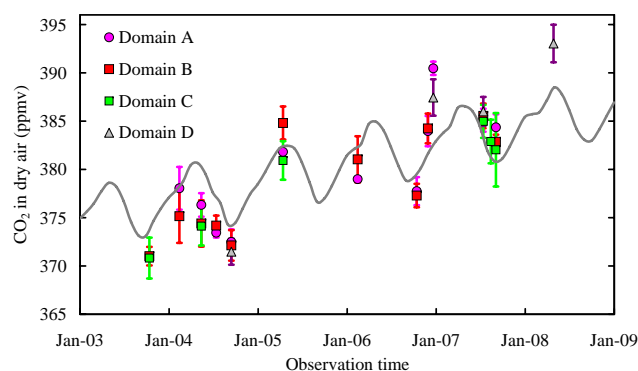


Fig. 5. Time series of field-measured atmospheric CO₂ concentrations at 10 m (mean \pm standard deviation in dry air) during the period from October 2003 to April 2008. A monthly mean data set for the Mauna Loa station (NOAA/ESRL, www.esrl.noaa.gov/gmd/ccgg/trends/) is also plotted as a grey curve.

represent the two largest sources of uncertainties in estimating regional sea–air CO₂ fluxes, i.e., the uncertainty introduced by $p\text{CO}_2$ interpolation and/or extrapolation and the

Table 5. Summary of $p\text{CO}_2$, salinity and SST along cruise tracks, monthly satellite-derived wind speed, and sea–air CO₂ flux estimation in domain C. The annual sea–air CO₂ flux amounts to $1.37 \pm 0.55 \text{ mol m}^{-2} \text{ yr}^{-1}$ using the S07 equation or $1.58 \pm 0.64 \text{ mol m}^{-2} \text{ yr}^{-1}$ using the W92 equation. Note that C2 and most errors in sea–air CO₂ flux estimation are the same as in Table 3. In winter, however, the error presented here was estimated based on the standard deviation of the wind speed, since only one cruise was available in this season. See text for details.

Observation time	Aqueous $p\text{CO}_2$ μatm	Air $p\text{CO}_2$ μatm	Salinity	SST $^\circ\text{C}$	Wind speed m s^{-1}	C2	Sea–air CO ₂ fluxes ($\text{mmol CO}_2 \text{ m}^{-2} \text{ d}^{-1}$)			
							Survey average (W92)	Seasonal average (W92)	Survey average (S07)	Seasonal average (S07)
1–11 Dec 2006	383 ± 5 (368–404)	No data (375*)	33.42 ± 0.19 (33.03–33.89)	27.7 ± 1.3 (24.14–28.96)	10.2 ± 1.4 (6.0–12.3)	1.12	2.18	2.2 ± 0.6 (winter)	1.90	1.9 ± 0.5 (winter)
May 2004	386 ± 7 (360–405)	356.5 ± 2.2 (350.9–362.8)	33.77 ± 0.15 (33.19–34.31)	29.6 ± 0.5 (27.65–30.65)	5.6 ± 0.5 (4.0–7.2)	1.38	3.10		2.70	
Apr 2005	412 ± 14 (383–463)	366.7 ± 2.2 (362.6–373.6)	33.89 ± 0.15 (33.48–34.33)	28.5 ± 0.4 (27.47–29.63)	5.1 ± 0.6 (4.1–7.6)	1.21	3.42	3.3 ± 0.3 (spring)	3.00	2.8 ± 0.2 (spring)
Jul 2007	404 ± 6 (393–415)	366.9 ± 2.1 (364.7–370.5)	34.02 ± 0.09 (33.70–34.11)	30.2 ± 0.3 (29.73–30.82)	6.6 ± 1.1 (4.4–9.1)	1.42	5.64		4.91	
Aug 2007	410 ± 14 (380–440)	364.5 ± 2.4 (360.5–369.3)	33.68 ± 0.24 (32.44–34.04)	28.3 ± 0.8 (25.89–30.25)	8.1 ± 1.3 (1.4–10.6)	1.30	9.58	7.6 ± 2.8 (summer)	8.35	6.6 ± 2.4 (summer)
Oct 2003	367 ± 9 (350–385)	354.7 ± 3.1 (349.1–361.6)	33.26 ± 0.47 (32.09–34.36)	29.4 ± 0.8 (27.58–30.47)	6.9 ± 1.2 (4.6–10.2)	1.35	1.85		1.62	
Sep 2007	404 ± 10 (376–436)	364.1 ± 3.8 (358.3–375.5)	32.49 ± 0.61 (30.56–33.68)	29.3 ± 0.5 (28.09–30.37)	6.7 ± 1.2 (4.2–11.5)	1.53	6.59	4.2 ± 3.4 (autumn)	5.74	3.7 ± 2.9 (autumn)

* The average of the mesan values measured in November 2006 and on 22–23 December 2006 in domain A (Table 3).

Table 6. Summary of $p\text{CO}_2$, salinity and SST along cruise tracks, monthly satellite-derived wind speed, and sea–air CO₂ flux estimation in domain D. The annual sea–air CO₂ flux amounts to $1.21 \pm 1.48 \text{ mol m}^{-2} \text{ yr}^{-1}$ using the S07 equation or $1.39 \pm 1.70 \text{ mol m}^{-2} \text{ yr}^{-1}$ using the W92 equation. Note that C2 and the error in sea–air CO₂ flux estimation in winter are the same as in Table 3. In the other seasons, however, the errors were estimated based on the standard deviation of the aqueous $p\text{CO}_2$, which primarily represented the spatial variation of aqueous $p\text{CO}_2$, since only one cruise was available in every season. See text for details.

Observation time	Aqueous $p\text{CO}_2$ μatm	Air $p\text{CO}_2$ μatm	Salinity	SST $^\circ\text{C}$	Wind speed m s^{-1}	C2	Sea–air CO ₂ fluxes ($\text{mmol CO}_2 \text{ m}^{-2} \text{ d}^{-1}$)			
							Survey average (W92)	Seasonal average (W92)	Survey average (S07)	Seasonal average (S07)
15–16 Dec 2006	367 ± 5 (357–379)	No data (375 ^a)	33.97 ± 0.17 (33.74–34.37)	25.2 ± 0.4 (24.55–25.83)	12.4 ± 1.0 (8.9–14.6)	1.05	–3.15		–2.74	
21–22 Dec 2006	410 ± 20 (379–469)	375.4 ± 2.9 (372.2–382.2)	34.01 ± 0.24 (33.50–34.47)	25.0 ± 0.9 (23.58–27.08)	$17.9 \pm 2.1^{\text{b}}$ (11.4–22.3)	1.04 ^b	28.5	12.7 ± 15.9 (winter)	24.8	11.0 ± 13.8 (winter)
Apr 2008	370 ± 13 (355–397)	378.6 ± 2.2 (374.0–382.7)	34.04 ± 0.13 (33.66–34.28)	27.9 ± 0.4 (26.82–28.72)	6.5 ± 0.8 (4.6–8.8)	1.34	–1.24	$–1.2 \pm 1.8$ (spring)	–1.08	$–1.1 \pm 1.5$ (spring)
Jul 2007	400 ± 6 (364–417)	366.5 ± 1.6 (363.5–370.4)	33.92 ± 0.16 (33.26–34.18)	30.3 ± 0.4 (29.38–31.65)	5.1 ± 0.4 (4.3–6.9)	1.38	2.95	2.9 ± 0.5 (summer)	2.57	2.6 ± 0.4 (summer)
Sep 2004	361 ± 3 (354–366)	356.8 ± 1.7 (354.2–359.9)	33.78 ± 0.22 (33.47–34.23)	28.9 ± 0.3 (28.41–29.50)	7.5 ± 0.5 (6.4–9.7)	1.39	0.86	0.9 ± 0.6 (autumn)	0.74	0.7 ± 0.5 (autumn)

^a The average of field-measured values on 21–22 December 2006 in domain D.

^b Based on field-measured wind speeds at 10 m height by the onboard weather station along the survey transect.

uncertainty introduced by environmental forcing parameters such as wind (Wanninkhof et al., 2009; Johnson et al., 2011).

In domain A, the sea area moderately absorbed CO₂ from the atmosphere in winter ($4.8 \pm 2.6 \text{ mmol m}^{-2} \text{ d}^{-1}$ using the S07 equation or $5.6 \pm 3.1 \text{ mmol m}^{-2} \text{ d}^{-1}$ using the W92 equation), while the sea–air CO₂ exchanges were nearly

in equilibrium in spring, summer, and autumn (Table 3). The annual sea–air CO₂ exchanges in this domain were nearly in equilibrium ($–0.44 \pm 0.65 \text{ mol m}^{-2} \text{ yr}^{-1}$ using the S07 equation or $–0.51 \pm 0.75 \text{ mol m}^{-2} \text{ yr}^{-1}$ using the W92 equation).

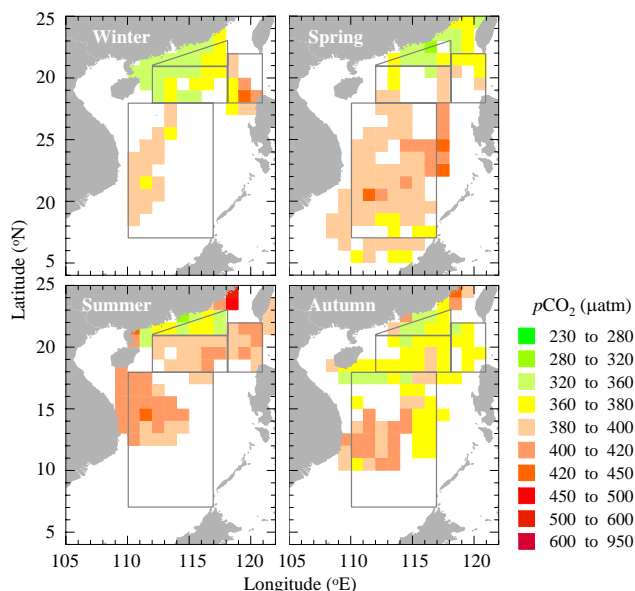


Fig. 6. Composite seasonal distributions of sea surface $p\text{CO}_2$ in the SCS proper during the period from October 2003 to April 2008 based on data presented in Fig. 2 and arithmetical averages over $1^\circ \times 1^\circ$ grid boxes.

In domain B, the sea–air CO₂ exchanges were nearly in equilibrium in winter and autumn, and the sea area released CO₂ into the atmosphere in spring ($1.7 \pm 0.8 \text{ mmol m}^{-2} \text{ d}^{-1}$ using the S07 equation or $1.9 \pm 1.0 \text{ mmol m}^{-2} \text{ d}^{-1}$ using the W92 equation) and summer ($3.2 \pm 0.3 \text{ mmol m}^{-2} \text{ d}^{-1}$ using the S07 equation or $3.7 \pm 0.3 \text{ mmol m}^{-2} \text{ d}^{-1}$ using the W92 equation) (Table 4). The annual sea–air CO₂ flux in domain B was estimated at $0.46 \pm 0.43 \text{ mol m}^{-2} \text{ yr}^{-1}$ using the S07 equation or $0.53 \pm 0.50 \text{ mol m}^{-2} \text{ yr}^{-1}$ using the W92 equation. In previous snapshot-based or time series station-based studies, researchers have estimated the northern SCS (i.e., domain B in this study) as a weak CO₂ source (approximately $0.86 \text{ mol m}^{-2} \text{ yr}^{-1}$ using the W92 equation) (Zhai et al., 2005a) or a very weak CO₂ sink with the absolute value of $0.19 \pm 0.19 \text{ mol m}^{-2} \text{ yr}^{-1}$ (Chou et al., 2005) or $0.02 \pm 1.06 \text{ mol m}^{-2} \text{ yr}^{-1}$ (Tseng et al., 2007) using the W92 equation. Our new multiple-year mapping results were roughly the median of all those previous results and basically supported the original idea that the SCS as a whole should serve as a weak source of atmospheric CO₂ (Zhai et al., 2005a; Chen et al., 2006; Dai et al., 2013).

Domain C released CO₂ into the atmosphere throughout the year (Table 5) with the survey-averaged sea–air CO₂ fluxes ranging from the low values of $1.62 \text{ mmol m}^{-2} \text{ d}^{-1}$ (using the S07 equation) in October 2003 (or $1.85 \text{ mmol m}^{-2} \text{ d}^{-1}$ using the W92 equation) and $1.90 \text{ mmol m}^{-2} \text{ d}^{-1}$ (using the S07 equation) in early December 2006 (or $2.20 \text{ mmol m}^{-2} \text{ d}^{-1}$ using the W92 equation) to a very high value of $8.35 \text{ mmol m}^{-2} \text{ d}^{-1}$ (using the S07 equation) in August 2007 (or $9.58 \text{ mmol m}^{-2} \text{ d}^{-1}$

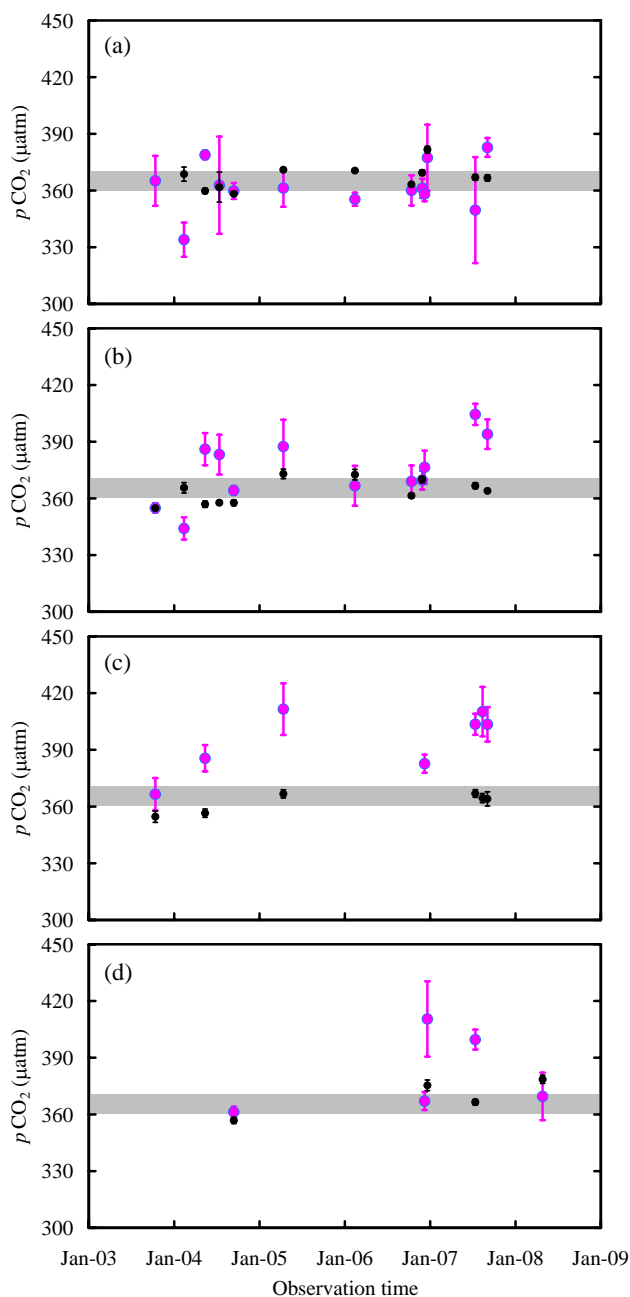


Fig. 7. Time series of field-measured sea surface $p\text{CO}_2$ (pink dots) and atmospheric $p\text{CO}_2$ (dark dots) for flux estimation in domain A (a), in domain B (b), in domain C (c), and in domain D (d) based on data presented in Tables 3, 4, 5, and 6. Data are shown as mean \pm standard deviation. The range of 360 to 370 μatm is marked by the grey band.

using the W92 equation). The annual sea–air CO₂ flux in domain C was estimated at $1.37 \pm 0.55 \text{ mol m}^{-2} \text{ yr}^{-1}$ using the S07 equation or $1.58 \pm 0.64 \text{ mol m}^{-2} \text{ yr}^{-1}$ using the W92 equation. Earlier, Rehder and Suess (2001) report their sea–air CO₂ flux estimates along the eastern

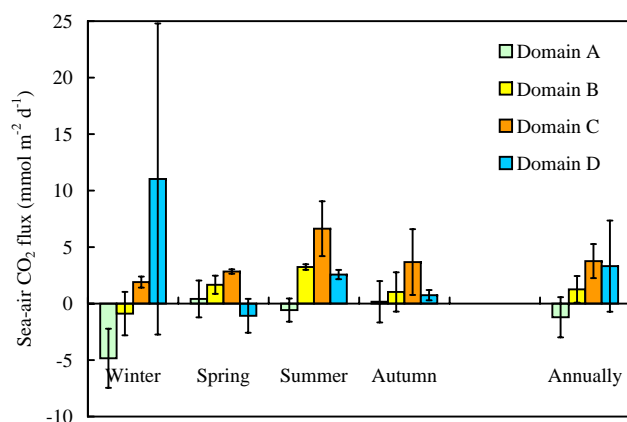


Fig. 8. Sea–air CO₂ flux estimation in four physical–biogeochemical domains in the South China Sea proper. Note that we used satellite-derived monthly averaged wind speeds and the Sweeney et al. (2007) equation (Eq. 1) to calculate gas transfer velocities and then sea–air CO₂ fluxes. Also shown are the “error” bars associated with each flux estimates, which were mostly attributable to intraseasonal variability. See text for details.

and southeastern boundaries of the SCS in September 1994 (0.55 to 1.40 $\text{mmol m}^{-2} \text{d}^{-1}$ using the W92 equation and the climatological wind in the month). Based on a summary of limited carbonate system data from the late 1990s and mass balance calculations, Chen et al. (2006) also suggested that the central/southern SCS basin area (i.e., domain C in this study) serves as a weak CO₂ source (0.73 $\text{mmol m}^{-2} \text{d}^{-1}$) in the wet season and a weaker CO₂ sink (-0.55 $\text{mmol m}^{-2} \text{d}^{-1}$) in the dry season. Our sea–air CO₂ flux estimates in domain C were much higher than all those previous results.

In domain D, the sea–air CO₂ exchanges varied from weak CO₂ uptake in spring (-1.1 ± 1.5 $\text{mmol m}^{-2} \text{d}^{-1}$ using the S07 equation or -1.2 ± 1.8 $\text{mmol m}^{-2} \text{d}^{-1}$ using the W92 equation) to weak or moderate CO₂ release in summer (2.6 ± 0.5 $\text{mmol m}^{-2} \text{d}^{-1}$ using the S07 equation or 2.9 ± 0.5 $\text{mmol m}^{-2} \text{d}^{-1}$ using the W92 equation), and were nearly in equilibrium with the atmosphere in autumn (Table 6). In winter, however, domain D varied very much from a typically weak CO₂ sink in early winter to a significant CO₂ source associated with a monsoon-driven upwelling event.

Overall, the seasonal pattern of sea–air CO₂ fluxes substantially differed among the four physical–biogeochemical domains under study. Although the annual sea–air CO₂ exchanges were nearly in equilibrium in domain A, most areas in the SCS proper served as weak to moderate sources to the atmospheric CO₂ on an annual basis (Fig. 8). With the four physical–biogeochemical domains under study taken together, it released 18 ± 10 Tg C yr^{-1} ($\text{Tg} = 10^{12}$ g) (based on the S07 equation) into the atmosphere. If we extrapolated such an average flux to the whole SCS proper (with the surface area of 2.5×10^6 km^2), we would derive a sea–air

CO₂ flux value of approximately 33.5 Tg C yr^{-1} . And thus the SCS proper, which represents 7.5 % of the surface area of global coastal oceans, accounts for 22 % of the CO₂ emission rate of the total 19 CO₂-releasing ocean margins (Dai et al., 2013). Considering this new result, the Dai et al. (2013) compilation value of the CO₂ sink in the global coastal ocean is slightly lowered by 5 % and updated to 0.34 Pg C yr^{-1} .

5 Discussion

5.1 Factors influencing sea surface pCO₂

In the oligotrophic northern SCS, it has been reported that temperature is the most important factor influencing the seasonal variation of sea surface pCO₂ (Zhai et al., 2005a; Tseng et al., 2007). According to Zhai et al. (2005a), the SST-driven pCO₂ values (in μatm) in the northern SCS vary in the range $(370 \pm 20) \times e^{0.0423(SST-26)}$, where 370 ± 20 is comparable to the range of local atmospheric pCO₂ (in μatm) at 10 m, 0.0423 $^{\circ}\text{C}^{-1}$ is the coefficient for the temperature effect of seawater pCO₂ (Takahashi et al., 1993), and 26 is comparable to the annual average SST (in $^{\circ}\text{C}$) in the offshore area of the northern SCS (Fig. 3a). In our study, however, we revealed a diverse relationship between pCO₂ and SST in the four different domains of the SCS proper as illustrated in Fig. 9. To further examine the pCO₂ control mechanism (especially in riverine/estuarine plumes), we also plotted temperature-normalized pCO₂ values (with the coefficient of 4.23 % $^{\circ}\text{C}^{-1}$ to a fixed temperature of 26 $^{\circ}\text{C}$) against salinity for domains A and C (Fig. 10).

In domain A, pCO₂ basically increased along with SST, although many pCO₂ values declined to the very low range of 280 to 320 μatm in the two summer cruises (Fig. 9a). Plots of temperature-normalized pCO₂ versus salinity (Fig. 10a) revealed that many of those summer data were associated with an estuarine plume (with a salinity of less than 33), where biological productivity was enhanced in the surface water due to nutrient support from the eutrophicated PRE (Cao et al., 2011; Han et al., 2012). Dai et al. (2008), Zhai et al. (2009), and Cao et al. (2011) have shown that the Pearl River plume can serve as a CO₂ sink. The plume-associated CO₂ consumption rates have been estimated as 36 ± 19 $\text{mmol C m}^{-2} \text{d}^{-1}$ in the shelf (Cao et al., 2011) or even 70 to 110 $\text{mmol C m}^{-2} \text{d}^{-1}$ in the limited sea area off the PRE (Dai et al., 2008). However, its influences were spatiotemporally limited depending on the river discharge (Figs. 2d–f; Dai et al., 2008; Zhai et al., 2009; Cao et al., 2011). In other river plumes with larger discharges such as the plume areas off the Changjiang Estuary (e.g., Zhai and Dai, 2009) and off the Amazon River (Ternon et al., 2000; Körtzinger, 2003; Cooley and Yager, 2006; Cooley et al., 2007), the uptakes of CO₂ are much more significant.

The winter coastal current along China coast added more complexities in domain A. For example, the plot of pCO₂

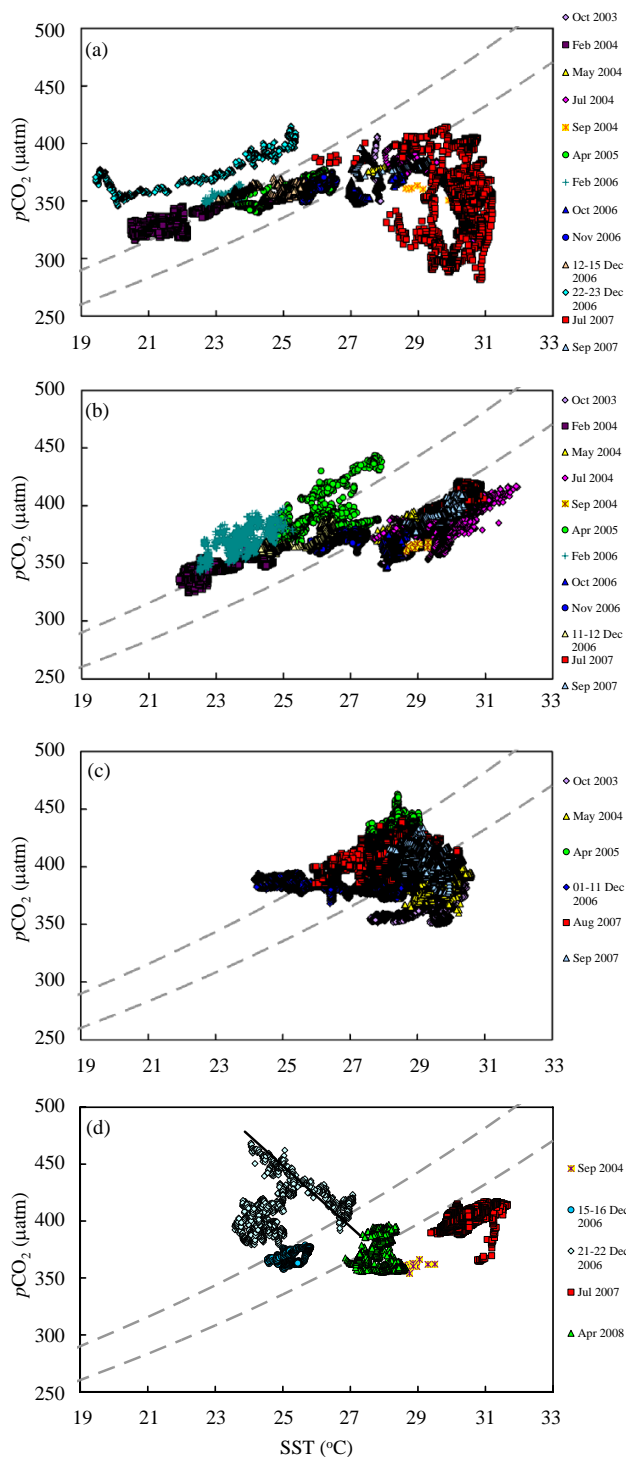


Fig. 9. Scatter plots of sea surface $p\text{CO}_2$ as a function of temperature in domain A (a), in domain B (b), in domain C (c), and in domain D (d). Dashed lines represent functions of $p\text{CO}_2 (\mu\text{atm}) = 390 e^{0.0423 (SST-26)}$ (the upper line) and of $p\text{CO}_2 (\mu\text{atm}) = 350 e^{0.0423 (SST-26)}$ (the lower line) according to Zhai et al. (2005a). In (d), the real line represents a function of $p\text{CO}_2 (\mu\text{atm}) = -26.737 \times \text{SST} (^{\circ}\text{C}) + 1116.9$ obtained during a neighboring study on 18–20 December 2006 according to Xu et al. (2009).

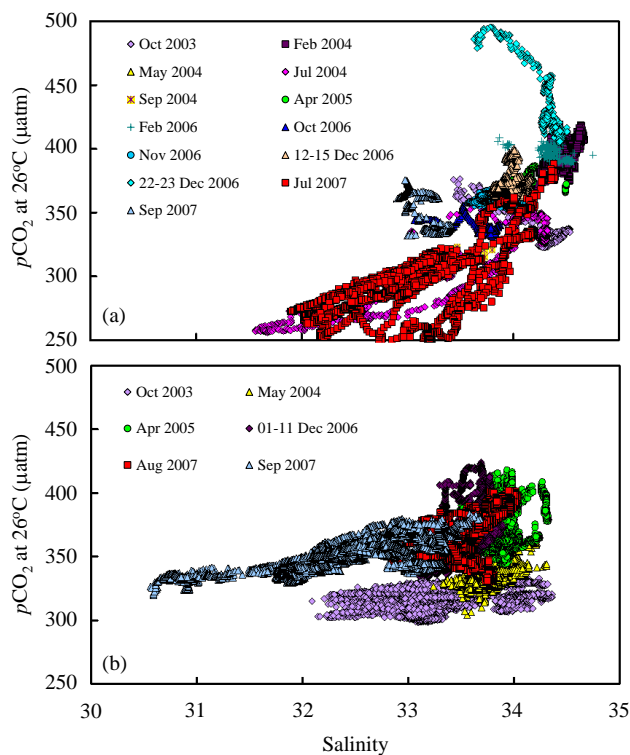


Fig. 10. Scatter plots of temperature-normalized $p\text{CO}_2$ as a function of salinity in domain A (a) and in domain C (b).

versus SST during the period 22–23 December 2006 was different from other winter plots in this region (Fig. 9a), and was even different from another data set obtained during the period 12–15 December 2006 (Fig. 9a) despite the small interval of only 7 to 10 days between the two surveys. Plots of temperature-normalized $p\text{CO}_2$ versus salinity (Fig. 10a) suggested that surface waters during the two December 2006 surveys might have originated from different water sources. Approximately four days before the 22–23 December 2006 survey, a strong northeast monsoon came in. The monsoon might have driven colder and $p\text{CO}_2$ -higher coastal waters from the Taiwan Strait into the northeastern part of domain A under survey (Fig. 2c). Similar monsoon-driven nutrient transport from the Taiwan Strait into the northeast SCS shelf was observed by Han et al. (2013).

Excluding the two July data sets and the 22–23 December 2006 data set, the other 10 surveys showed a linear positive correlation between $p\text{CO}_2$ and SST in domain A (Fig. 9a). In cold seasons the field-measured $p\text{CO}_2$ data were slightly higher than the predicted values based on thermodynamically controlling functions, while in warm seasons relatively lower $p\text{CO}_2$ values were measured (Fig. 9a). Moreover, temperature-normalized $p\text{CO}_2$ during these 10 surveys showed a clear seasonal cycle in the water mass with a salinity higher than 33.5 (Fig. 10a). The typical temperature-normalized $p\text{CO}_2$ (at 26°C) ranged between

380 and 420 μatm in the winter cruises, while in the warm seasons most of the temperature-normalized $p\text{CO}_2$ (at 26 °C) ranged from 330 to 370 μatm (Fig. 10a). The former (relatively higher than atmospheric equilibrated level) might have resulted from enhanced water mixing between surface water and CO₂-rich subsurface waters in winter. The latter (atmospheric equilibrated level or less) might have originated from CO₂ degassing of the surface water for several months following stratification enhancement in spring.

In domain B, most plots of $p\text{CO}_2$ versus temperature were similar to those in the high-salinity areas in domain A, although the field-measured $p\text{CO}_2$ data during April 2005 surveys were slightly higher than those predicted based on thermodynamically controlling lines (Fig. 9b). The SST data measured during the April 2005 surveys were significantly lower than those obtained in May 2004 (26.3 ± 0.9 °C vs. 28.6 ± 0.8 °C, Table 4), suggesting that they might have been influenced by a vertical mixing event in early spring. Figure 9b indeed suggested that many April 2005 data followed the same thermodynamically controlling line as the two February (in winter) data sets. The relationships between temperature-normalized $p\text{CO}_2$ and salinity were random in domain B (plot not reported).

In domain C, the influences of SST on $p\text{CO}_2$ showed no clear trend, although a weakly negative correlation of $p\text{CO}_2$ and SST and a positive correlation of temperature-normalized $p\text{CO}_2$ versus salinity were observed in the southwestern SCS on September 2007 (Figs. 9c and 10b). During the late August and early September surveys in 2007, the influence of MKRDW was coupled with two offshore cold eddies in the southwestern SCS (Chen et al., 2010). According to Chen et al. (2010), the MKRDW was identified with a salinity less than 33.2 and an SST higher than 29.0 °C during the September 2007 survey, while the two cold eddies had a relatively high salinity of > 33.2 and a relatively low SST of ~ 28.2 °C at the center. Figure 9c shows that both the highest $p\text{CO}_2$ value (~ 430 μatm) and the lowest $p\text{CO}_2$ value (~ 380 μatm) during the September 2007 survey were observed in the MKRDW area. In the September eddy (eddy II in Chen et al. 2010), a relatively narrow $p\text{CO}_2$ range of 393 to 423 μatm (Fig. 9c) was observed. In the August eddy (eddy I in Chen et al. 2010), however, a relatively wide $p\text{CO}_2$ range of 383 to 440 μatm (Fig. 9c) was revealed. Figure 10b suggests that three-endmember water mixing occurred in the southwestern SCS in both late summer and early autumn. The low-salinity MKRDW was identified with a relatively low temperature-normalized $p\text{CO}_2$ (at 26 °C) of 320 to 340 μatm (Fig. 10b). The high-salinity area (with a salinity higher than 33.2) was influenced by two water end members. One had the similar temperature-normalized (at 26 °C) $p\text{CO}_2$ values of 330 to 345 μatm as the MKRDW. Another high-salinity water mass was identified with relatively low SST (Chen et al., 2010) but significantly high temperature-normalized (at 26 °C) $p\text{CO}_2$ values of 375 to 400 μatm (Fig. 10b), which were influenced by cold eddies,

similar to the phenomenon observed in the lee of the main Hawaiian islands (Chen et al., 2007b). Detailed influences of the two cold eddies on sea–air CO₂ fluxes in the southwestern SCS in late summer and early autumn will be addressed elsewhere.

In domain C, if the influences of the MKRDW and cold eddies were excluded, the seasonal temperature-normalized (at 26 °C) $p\text{CO}_2$ varied from 300–330 μatm in October 2003 (autumn) to 345–418 μatm in April 2005 (early spring) and 335–425 μatm in December 2006 (early winter) (Fig. 10b). This seasonal cycle of temperature-normalized $p\text{CO}_2$ might also have resulted from enhanced water mixing between surface water and CO₂-rich subsurface waters in winter/early spring and the CO₂ degassing of the surface water for several months following stratification enhancement in spring.

In domain D, a negative relationship between $p\text{CO}_2$ and SST was observed during the 21–22 December 2006 survey (Fig. 9d). Two days before our survey, Xu et al. (2009) observed a similar phenomenon in the sea surface on the adjacent coast. Based on multiple comparisons of temperature, salinity, and nutrient concentrations, they conclude that the low-temperature (~ 24 °C) water with a high- $p\text{CO}_2$ (~ 460 μatm) level is upwelled from the 45 to 80 m depth (Xu et al., 2009). Actually, the strong northeast monsoon came in three days before the 21–22 December 2006 survey. Even when the monsoon had weakened, a strong northeast wind (17.9 ± 2.1 m s^{-1} during our two-day survey versus 9.8 ± 2.0 m s^{-1} before the event) was observed. Based on satellite-derived SST images (Tropical Rainfall Measuring Mission – Microwave Imager) on 22–23 December 2006, a relatively cold (~ 22 °C versus the neighboring 25.0 ± 0.9 °C) area was revealed between 18°30' and 20°00' N and 118°30' and 120°30' E (C.-Y. Zhang, unpublished data), indicating that upwelling might occur, which resulted in the negative relationship between $p\text{CO}_2$ and SST, and thus a significant CO₂ degassing event.

The CO₂ effects of this monsoon-driven offshore upwelling were comparable to the nearby coastal upwelling reported by Xu et al. (2009). Similar peak levels of the offshore high $p\text{CO}_2$ were revealed to be 460 to 470 μatm by Xu et al. (2009) and in this study (Fig. 9d). Since the strong northeast monsoon drove the climatologically cold eddy in the western Luzon Strait in winter (Shang et al., 2012), the wintertime CO₂ degassing events might have contributed to the seasonal characteristics of sea–air CO₂ exchange in this region. However, this winter sea–air CO₂ exchange was subject to large variability due to rapid CO₂ degassing and subsequent sea surface primary production driven by upwelled nutrients from the subsurface waters. In January 2010, Shang et al. (2012) note intensive phytoplankton blooms in the Luzon Strait and its vicinity. The associated sea surface $p\text{CO}_2$ at this time was 10 to 20 μatm lower than the atmospheric equilibrated level (M.-H. Dai et al., unpublished data).

In summary, besides the general pattern of temperature-induced seasonal variation of sea surface $p\text{CO}_2$ in the SCS,

the influences of river plume with low $p\text{CO}_2$, water mixing between surface water and CO₂-rich subsurface waters in cold seasons, CO₂ degassing from the surface water in warm seasons, and episodic events of eddy and upwelling around the SCS also impose high variability on surface $p\text{CO}_2$ distribution, as well as sea–air CO₂ flux estimation.

5.2 Impact of winter-monsoon-induced events of CO₂ degassing on the annual sea–air CO₂ flux

Most of the above-discussed data sets reflected normal variations in the respective domains. It must be pointed out, however, that many episodic events might significantly impact on the CO₂ fluxes. An example is the winter-monsoon-induced CO₂ degassing event observed in domain D in late December 2006 described above. As shown in Table 6, the area-averaged sea–air CO₂ fluxes increased by $\sim 27 \text{ mmol m}^{-2} \text{ d}^{-1}$ within a time lag of one week due to upwelling of the subsurface water. This change was much greater than a similar phenomenon in spring in the lee of the main Hawaiian islands (Chen et al., 2007b) but was similar to that observed in equatorial upwelling areas in the eastern Pacific (Chavez et al., 1999). To further evaluate the amount of CO₂ released during this event, we assumed that the Revelle factor (RF) of the upwelled water was ~ 10 , the $\text{DIC}_{\text{avg}} \sim 2000 \mu\text{mol L}^{-1}$, the aqueous $p\text{CO}_{2,\text{avg}} \sim 410 \mu\text{atm}$, and the air-saturated $p\text{CO}_2 \sim 375 \mu\text{atm}$. Based on the eloquent definition of RF given by Sundquist et al. (1979), the oversaturated and then releasable DIC could therefore be estimated via $\Delta\text{DIC} = \Delta p\text{CO}_2 / p\text{CO}_{2,\text{avg}} / \text{RF} \times \text{DIC}_{\text{avg}} = (410 - 375) / 410 / 10 \times 2000 = 17 \mu\text{mol L}^{-1}$. Given that the upper mixed layer depth was 45 to 80 m (Xu et al., 2009), the eddy-related CO₂ release should be 0.76 to 1.36 mol m^{-2} . This was comparable with the annual CO₂ release in domain D (Fig. 8).

This case showed that the very strong winter monsoon not only caused a high gas transfer velocity but also enhanced vertical water mixing. When the CO₂-rich subsurface water is mixed with the surface water, a winter CO₂ sink area in the subtropical ocean might be reversed into a winter source area. Due to surveying difficulties, very few cases of winter CO₂ source events are found in the winter CO₂ sink database. In such a case, if we neglected the CO₂ variability due to monsoon-induced eddies, the annually based sea–air CO₂ flux would be nearly zero (Table 6). Thus, the winter-monsoon-induced CO₂ degassing events had substantial impacts on the annually based sea–air CO₂ fluxes. This issue clearly needs further investigation despite the difficulties in observation.

6 Concluding remarks

This study has clearly shown that neither snapshot-based nor time series station-based investigations were sufficient to adequately assess sea–air CO₂ fluxes in an ocean margin that is often characterized by tremendous dynamic environments. In the largest tropical marginal sea, the SCS, this research was the first attempt to simultaneously resolve both spatial and seasonal coverages. We analyzed the temporal–spatial variations and the controlling mechanisms of sea surface $p\text{CO}_2$ in the SCS proper. We also estimated the sea–air CO₂ fluxes and their temporal–spatial variability based on 14 mapping cruises. We demonstrated once more that the SCS as a whole serves as a weak to moderate source of atmospheric CO₂ (Zhai et al., 2005a; Chen et al., 2006; Dai et al., 2013), although the $p\text{CO}_2$ variability in the SCS proper was remarkable both in time and space, and the critical roles of wind speed variability and the gas transfer velocity in the annual sea–air CO₂ flux estimation were still unresolved.

Acknowledgements. We thank Yi Wang, Gui Chen, Zhaozhang Chen, Ke Liu, Benwang Wang, and Zhimian Cao for assistance in the data collection during several cruises, Zhongming Lu for sharing the February 2006 $p\text{CO}_2$ data set around the Xisha Islands, and Professor John Hodgkiss for his assistance with English. Jiwei Tian, Pinghe Cai and the crews of R/V *Shiyan 3*, R/V *Dongfanghong 2*, R/V *Yanping 2*, R/V *Kexue 3*, and R/V *Haijian 83* provided much help during the sampling cruises. Valuable comments from Christophe Rabouille, Wiley Evans, and an anonymous reviewer have improved the quality of the manuscript. The research was jointly supported by the National Basic Research Program of China (2009CB421201), the National Natural Science Foundation of China (NSFC) (41130857, 41121091, 41206061, 41076044, and 90711005), and the State Oceanic Administration of China (SOA) (contract DOMEPA-MEA-01-10). Sampling surveys were partially supported by the NSFC (90211020, 40490264, and 40521003) using R/V *Yanping 2* and R/V *Dongfanghong 2*; the South China Sea Institute of Oceanology (SCSIO, CAS, China) via the Integrated Nansha Scientific Investigation Cruise 2004, and via the South China Sea Open Cruise 2004 using R/V *Shiyan 3*; the National High-Tech Research and Development Program (“863” Program) of China via the project of Quality Control/in situ Standardization Experiment 2007 using R/V *Dongfanghong 2*; the Institute of Oceanology, CAS, China, via the China Sea Open Cruise 2006 using R/V *Kexue 3*; and the SOA via the South China Sea Repeat Section Investigation in winter 2006 using R/V *Haijian 83*.

Edited by: C. Rabouille

References

- Bates, N. R. and Merlivat, L.: The influence of short-term wind variability on air–sea CO₂ exchange, *Geophys. Res. Lett.*, 28, 3281–3284, 2001.
- Borges, A. V.: Present day carbon dioxide fluxes in the coastal ocean and possible feedbacks under global change, In: *Oceans and the*

- Atmospheric Carbon Content, edited by: Duarte, P. and Santana-Casiano, J. M., Berlin, Springer, 47–77, 2011.
- Borges, A. V., Delille, B., and Frankignoulle, M.: Budgeting sinks and sources of CO₂ in the coastal ocean: diversity of ecosystems counts, *Geophys. Res. Lett.*, 32, L14601, doi:10.1029/2005GL023053, 2005.
- Cai, W.-J.: Estuarine and coastal ocean carbon paradox: CO₂ sinks or sites of terrestrial carbon incineration?, *Annu. Rev. Mar. Sci.*, 3, 123–145, 2011.
- Cai, W.-J., Dai, M.-H., and Wang, Y.-C.: Air-sea exchange of carbon dioxide in ocean margins: A province-based synthesis, *Geophys. Res. Lett.*, 33, L12603, doi:10.1029/2006GL026219, 2006.
- Cao, Z.-M., Dai, M.-H., Zheng, N., Wang, D.-L., Li, Q., Zhai, W.-D., Meng, F.-F., and Gan, J.-P.: Dynamics of the carbonate system in a large continental shelf system under the influence of both a river plume and coastal upwelling, *J. Geophys. Res.*, 116, G02010, doi:10.1029/2010JG001596, 2011.
- Chavez, F. P., Strutton, P. G., Friederich, G. E., Feely, R. A., Feldman, G. C., Foley, D. G., and McPhaden, M. J.: Biological and chemical response of the equatorial Pacific Ocean to the 1997–98 El Niño, *Science*, 286, 2126–2131, 1999.
- Chen, C.-T. A. and Borges, A. V.: Reconciling opposing views on carbon cycling in the coastal ocean: continental shelves as sinks and near-shore ecosystems as sources of atmospheric CO₂, *Deep-Sea Res. Pt. II*, 56, 578–590, 2009.
- Chen, C.-T. A., Wang, S.-L., Wang, B.-J., and Pai, S.-C.: Nutrient budgets for the South China Sea basin, *Mar. Chem.*, 75, 281–300, 2001.
- Chen, C.-T. A., Wang, S.-L., Chou, W.-C., and Sheu, D.-D.: Carbonate chemistry and projected future changes in pH and CaCO₃ saturation state of the South China Sea, *Mar. Chem.*, 101, 277–305, 2006.
- Chen, F.-Z., Cai, W.-J., Benitez-Nelson, C., and Wang, Y.-C.: Sea surface pCO₂-SST relationships across a cold-core cyclonic eddy: Implications for understanding regional variability and air-sea gas exchange, *Geophys. Res. Lett.*, 34, L10603, doi:10.1029/2006GL028058, 2007b.
- Chen, W.-F., Liu, Q., Huh, C.-A., Dai, M.-H., and Miao, Y.-C.: Signature of the Mekong River plume in the western South China Sea revealed by radium isotopes, *J. Geophys. Res.*, 115, C12002, doi:10.1029/2010JC006460, 2010.
- Chen, Y.-L. L. and Chen, H.-Y.: Seasonal dynamics of primary and new production in the northern South China Sea: the significance of river discharge and nutrient advection, *Deep-Sea Res. Pt. I*, 53, 971–986, 2006.
- Chen, Y.-L. L., Chen, H.-Y., Lin, I.-I., Lee, M.-A., and Chang, J.: Effects of cold eddy on phytoplankton production and assemblages in Luzon Strait bordering the South China Sea, *J. Oceanogr.*, 63, 671–683, 2007a.
- Chou, W.-C., Sheu, D.-D., Chen, C.-T. A., Wang, S.-L., and Tseng, C.-M.: Seasonal variability of carbon chemistry at the SEATS time-series site, northern South China Sea between 2002 and 2003, *Terr. Atmos. Ocean. Sci.*, 16, 445–465, 2005.
- Cooley, S. R., Coles, V. J., Subramaniam, A., and Yager, P. L.: Seasonal variations in the Amazon plume-related atmospheric carbon sink, *Global Biogeochem. Cy.*, 21, GB3014, doi:10.1029/2006GB002831, 2007.
- Cooley, S. R. and Yager, P. L.: Physical and biological contributions to the western tropical North Atlantic Ocean carbon sink formed by the Amazon River plume, *J. Geophys. Res.*, 111, C08018, doi:10.1029/2005JC002954, 2006.
- Dai, M.-H., Cao, Z.-M., Guo, X.-H., Zhai, W.-D., Liu, Z.-Y., Yin, Z.-Q., Xu, Y.-P., Gan, J.-P., Hu, J.-Y., and Du, C.-J.: Why are some marginal seas sources of atmospheric CO₂?, *Geophys. Res. Lett.*, 40, 2154–2158, doi:10.1002/grl.50390, 2013.
- Dai, M.-H., Lu, Z.-M., Zhai, W.-D., Chen, B.-S., Cao, Z.-M., Zhou, K.-B., Cai, W.-J., and Chen, C.-T. A.: Diurnal variations of surface seawater pCO₂ in contrasting coastal environments, *Limnol. Oceanogr.*, 54, 735–745, 2009.
- Dai, M.-H., Zhai, W.-D., Cai, W.-J., Callahan, J., Huang, B.-Q., Shang, S.-L., Huang, T., Li, X.-L., Lu, Z.-M., Chen, W.-F., and Chen, Z.-Z.: Effects of an estuarine plume-associated bloom on the carbonate system in the lower reaches of the Pearl River estuary and the coastal zone of the northern South China Sea, *Cont. Shelf Res.*, 28, 1416–1423, 2008.
- Du, C., Liu, Z., Dai, M., Kao, S.-J., Cao, Z., Zhang, Y., Huang, T., Wang, L., and Li, Y.: Impact of the Kuroshio intrusion on the nutrient inventory in the upper northern South China Sea: insights from an isopycnal mixing model, *Biogeosciences*, 10, 6419–6432, doi:10.5194/bg-10-6419-2013, 2013.
- Gan, J.-P., Li, L., Wang, D.-X., and Guo, X.-G.: Interaction of a river plume with coastal upwelling in the northeastern South China Sea, *Cont. Shelf Res.*, 29, 728–740, 2009.
- Griessbaum, F., Moat, B. I., Narita, Y., Yelland, M. J., Klemm, O., and Uematsu, M.: Uncertainties in wind speed dependent CO₂ transfer velocities due to airflow distortion at anemometer sites on ships, *Atmos. Chem. Phys.*, 10, 5123–5133, doi:10.5194/acp-10-5123-2010, 2010.
- Han, A., Dai, M., Gan, J., Kao, S.-J., Zhao, X., Jan, S., Li, Q., Lin, H., Chen, C.-T. A., Wang, L., Hu, J., Wang, L., and Gong, F.: Inter-shelf nutrient transport from the East China Sea as a major nutrient source supporting winter primary production on the northeast South China Sea shelf, *Biogeosciences Discuss.*, 10, 3891–3923, doi:10.5194/bgd-10-3891-2013, 2013.
- Han, A.-Q., Dai, M.-H., Kao, S.-J., Gan, J.-P., Li, Q., Wang, L.-F., Zhai, W.-D., and Wang, L.: Nutrient dynamics and biological consumption in a large continental shelf system under the influence of both a river plume and coastal upwelling, *Limnol. Oceanogr.*, 57, 486–502, 2012.
- Han, W.-Y.: *Marine Chemistry in the South China Sea*, Beijing, Science Press, 289 pp., 1998 (in Chinese).
- Hu, J.-Y., Gan, J.-P., Sun, Z.-Y., Zhu, J., and Dai, M.-H.: Observed three-dimensional structure of a cold eddy in the southwestern South China Sea, *J. Geophys. Res.*, 116, C05016, doi:10.1029/2010JC006810, 2011.
- Jiang, L.-Q., Cai, W.-J., Wanninkhof, R., Wang, Y.-C., and Lüger, H.: Air–sea CO₂ fluxes on the U.S. South Atlantic Bight: Spatial and seasonal variability, *J. Geophys. Res.*, 113, C07019, doi:10.1029/2007JC004366, 2008.
- Jo, Y.-H., Dai, M.-H., Zhai, W.-D., Yan, X.-H., and Shang, S.-L.: On the variations of sea surface pCO₂ in the northern South China Sea: A remote sensing based neural network approach, *J. Geophys. Res.*, 117, C08022, doi:10.1029/2011JC007745, 2012.
- Johnson, M. T., Hughes, C., Bell, T. G., and Liss, P. S.: A Rumsfeldian analysis of uncertainty in air-sea gas exchange, in: *Gas Transfer at Water Surfaces*, Kyoto University Press, 464–485, 2011.

- Körtzinger, A.: A significant CO₂ sink in the tropical Atlantic Ocean associated with the Amazon River plume, *Geophys. Res. Lett.*, 30, 2287, doi:10.1029/2003GL018841, 2003.
- Laruelle, G. G., Dürr, H. H., Slomp, C. P., and Borges, A. V.: Evaluation of sinks and sources of CO₂ in the global coastal ocean using a spatially explicit typology of estuaries and continental shelves, *Geophys. Res. Lett.*, 37, L15607, doi:10.1029/2010GL043691, 2010.
- Li, L., Nowlin, W., and Su, J.-L.: Anticyclonic rings from the Kuroshio in the South China Sea, *Deep-Sea Res. Pt. I*, 45, 1469–1482, 1998.
- Liu, K.-K., Atkinson, L., Quiñones, R. A., and Talaue-McManus, L.: Biogeochemistry of continental margins in a global context, in: *Carbon and Nutrient Fluxes in Continental Margins – A Global Synthesis*, edited by: Liu, K.-K., Atkinson, L., Quiñones, R., and Talaue-McManus, L., Berlin, Springer, 3–24, 2010.
- Ning, X., Chai, F., Xue, H., Cai, Y., Liu, C., and Shi, J.: Physical-biological oceanographic coupling influencing phytoplankton and primary production in the South China Sea, *J. Geophys. Res.*, 109, C10005, doi:10.1029/2004JC002365, 2004.
- Rehder, G. and Suess, E.: Methane and pCO₂ in the Kuroshio and the South China Sea during maximum summer surface temperatures, *Mar. Chem.*, 75, 89–109, 2001.
- Sasai, Y., Sasaki, H., and Richards, K. J.: Impact of physical processes on the phytoplankton blooms in the South China Sea: an eddy-resolving physical-biological model study, *Biogeosciences Discuss.*, 10, 1577–1604, doi:10.5194/bgd-10-1577-2013, 2013.
- Shang, S.-L., Li, L., Li, J., Li, Y.-H., Lin, G., and Sun, J.: Phytoplankton bloom during the northeast monsoon in the Luzon Strait bordering the Kuroshio, *Remote Sens. Environ.*, 124, 38–48, 2012.
- Sheu, W.-J., Wu, C.-R., and Oey, L.-Y.: Blocking and westward passage of eddies in the Luzon Strait, *Deep-Sea Res. Pt. II*, 57, 1783–1791, 2010a.
- Sheu, D.-D., Chou, W.-C., Wei, C.-L., Hou, W.-P., Wong, G. T. F., and Hsu, C.-W.: Influence of El Niño on the sea-to-air CO₂ flux at the SEATS time-series site, northern South China Sea, *J. Geophys. Res.*, 115, C10021, doi:10.1029/2009JC006013, 2010b.
- Smith, S. V. and Hollibaugh, J. T.: Coastal metabolism and the oceanic organic carbon balance, *Rev. Geophys.*, 31, 75–89, 1993.
- Sundquist, E. T., Plummer, L. N., and Wigley, T. M. L.: Carbon dioxide in the ocean surface: the homogenous buffer factor, *Science*, 204, 1203–1205, 1979.
- Sweeney, C., Gloor, E., Jacobson, A. R., Key, R. M., McKinley, G., Sarmiento, J. L., and Wanninkhof, R.: Constraining global air-sea gas exchange for CO₂ with recent bomb ¹⁴C measurements, *Global Biogeochem. Cy.*, 21, GB2015, doi:10.1029/2006GB002784, 2007.
- Takahashi, T., Olafsson, J., Goddard, J. G., Chipman, D. W., and Sutherland, S. C.: Seasonal variation of CO₂ and nutrients in the high-latitude surface oceans: a comparative study, *Global Biogeochem. Cy.*, 7, 843–878, 1993.
- Tan, S.-C. and Shi, G.-Y.: Spatiotemporal variability of satellite-derived primary production in the South China Sea, 1998–2006, *J. Geophys. Res.*, 114, G03015, doi:10.1029/2008JG000854, 2009.
- Ternon, J. F., Oudot, C., Dessier, A., and Diverres, D.: A seasonal tropical sink for atmospheric CO₂ in the Atlantic Ocean: the role of the Amazon River discharge, *Mar. Chem.*, 68, 183–201, 2000.
- Tseng, C.-M., Wong, G. T. F., Chou, W.-C., Lee, B.-S., Sheu, D.-D., and Liu, K.-K.: Temporal variations in the carbonate system in the upper layer at the SEATS station, *Deep-Sea Res. Pt. II*, 54, 1448–1468, 2007.
- Tsunogai, S., Watanabe, S., and Sato, T.: Is there a “continental shelf pump” for the absorption of atmospheric CO₂?, *Tellus B*, 51, 701–712, 1999.
- Walsh, J. J., Rowe, G. T., Iverson, R. L., and McRoy, C. P.: Biological export of shelf carbon is a sink of the global CO₂ cycle, *Nature*, 291, 196–201, 1981.
- Wanninkhof, R., Asher, W. E., Ho, D. T., Sweeney, C., and McGillis, W. R.: Advances in quantifying air-sea gas exchange and environmental forcing, *Annu. Rev. Mar. Sci.*, 1, 213–244, 2009.
- Wanninkhof, R.: Relationship between wind-speed and gas-exchange over the ocean, *J. Geophys. Res.*, 97, 7373–7382, 1992.
- Weiss, R. F. and Price, R. A.: Nitrous oxide solubility in water and seawater, *Mar. Chem.*, 8, 347–359, 1980.
- Weiss, R. F.: Carbon dioxide in water and seawater: the solubility of a non-ideal gas, *Mar. Chem.*, 2, 203–215, 1974.
- Wong, G. T. F., Ku, T.-L., Mulholland, M., Tseng, C.-M., and Wang, D.-P.: The SouthEast Asian Time-series Study (SEATS) and the biogeochemistry of the South China Sea: an overview, *Deep-Sea Res. Pt. II*, 54, 1434–1447, 2007.
- Xu, Y.-P., Dai, M.-H., Zhai, W.-D., Yuan, D.-X., Liu, J.-W., Sun, Z.-Y., Lin, H., and Wu, J.-Y.: Short-term dynamics of nutrients influenced by upwelling in a small oligotrophic coastal ecosystem, Gan Bay, in the northwest Philippines, *Prog. Nat. Sci.*, 19, 595–601, 2009.
- Yan, H.-Q., Yu, K.-F., Shi, Q., Tan, Y.-H., Zhang, H.-L., Zhao, M.-X., Li, S., Chen, T.-R., Huang, L.-Y., and Wang, P.-X.: Coral reef ecosystems in the South China Sea as a source of atmospheric CO₂ in summer, *Chinese Sci. Bull.*, 56, 676–684, 2011.
- Yuan, Y.-L., Zheng, Q.-A., Dai, D.-J., Hu, X.-M., Qiao, F.-L., and Meng, J.-M.: Mechanism of internal waves in the Luzon Strait, *J. Geophys. Res.*, 111, C11S17, doi:10.1029/2005JC003198, 2006.
- Zhai, W.-D. and Dai, M.-H.: On the seasonal variation of air-sea CO₂ fluxes in the outer Changjiang (Yangtze River) Estuary, East China Sea, *Mar. Chem.*, 117, 2–10, 2009.
- Zhai, W.-D., Dai, M.-H., Cai, W.-J., Wang, Y.-C., and Hong, H.-S.: The partial pressure of carbon dioxide and air-sea fluxes in the northern South China Sea in spring, summer and autumn, *Mar. Chem.*, 96, 87–97, 2005a [Erratum: *Mar. Chem.*, 103, 209, 2007].
- Zhai, W.-D., Dai, M.-H., Cai, W.-J., Wang, Y.-C., and Wang, Z.-H.: High partial pressure of CO₂ and its maintaining mechanism in a subtropical estuary: the Pearl River estuary, China, *Mar. Chem.*, 93, 21–32, 2005b.
- Zhai, W. D., Dai, M., and Cai, W.-J.: Coupling of surface pCO₂ and dissolved oxygen in the northern South China Sea: impacts of contrasting coastal processes, *Biogeosciences*, 6, 2589–2598, doi:10.5194/bg-6-2589-2009, 2009.